

Invited Research Article

Cold-water corals as archives of seawater Zn and Cu isotopes

Susan H. Little^{a,b,*}, David J. Wilson^a, Mark Rehkämper^b, Jess F. Adkins^c, Laura F. Robinson^d, Tina van de Flierdt^b^a Department of Earth Sciences, University College London, Gower Place, London WC1E 6BS, UK^b Department of Earth Science and Engineering, Royal School of Mines, Imperial College London, London SW7 2BP, UK^c Division of Geological and Planetary Sciences, California Institute of Technology, Pasadena, CA 91125, USA^d School of Earth Sciences, University of Bristol, Bristol BS8 1RJ, UK

ARTICLE INFO

Editor: Michael E. Boettcher

Keywords:

Cold-water coral
Zinc
Copper
Isotopes
Aragonites
Palaeoceanography

ABSTRACT

Traditional carbonate sedimentary archives have proven challenging to exploit for Zn and Cu isotopes, due to the high concentrations of trace metals in potential contaminants (e.g., Fe-Mn coatings) and their low concentrations in carbonate. Here, we present the first dataset of $\delta^{66}\text{Zn}_{\text{JMC-Lyon}}$ and $\delta^{65}\text{Cu}_{\text{SRM 976}}$ values for cold-water corals and address their potential as a seawater archive. Extensive cleaning experiments carried out on two corals with well-developed Fe-Mn rich coatings demonstrate that thorough physical and chemical cleaning can effectively remove detrital and authigenic contaminants. Next, we present metal/Ca ratios and $\delta^{66}\text{Zn}$ and $\delta^{65}\text{Cu}$ values for a geographically diverse sample set of Holocene age cold-water corals. Comparing cold-water coral $\delta^{66}\text{Zn}$ values to estimated ambient seawater $\delta^{66}\text{Zn}$ values (where $\Delta^{66}\text{Zn}_{\text{coral-sw}} = \delta^{66}\text{Zn}_{\text{coral}} - \delta^{66}\text{Zn}_{\text{seawater}}$), we find $\Delta^{66}\text{Zn}_{\text{coral-sw}} = +0.03 \pm 0.17\text{‰}$ (1SD, $n = 20$). Hence, to a first order, cold-water corals record seawater Zn isotope compositions without fractionation. The average Holocene coral Cu isotope composition is $+0.59 \pm 0.23\text{‰}$ (1SD, $n = 15$), similar to the mean of published deep seawater $\delta^{65}\text{Cu}$ values at $+0.66 \pm 0.09\text{‰}$, but with considerable variability. Finally, $\delta^{66}\text{Zn}$ and $\delta^{65}\text{Cu}$ data are presented for a small subset of four glacial-age corals. These values overlap with the respective Holocene coral datasets, hinting at limited glacial-interglacial changes in oceanic Zn and Cu cycling.

1. Introduction

Zinc (Zn) and copper (Cu) are bioessential trace metals with isotopic systems that are emerging as promising tracers of past ocean nutrient and redox cycling. To date, reliable archives for past seawater Zn and Cu isotopes have been lacking, because both metals are present at low concentrations in carbonate and opal, but at high concentrations in potential contaminating material, such as detrital or authigenic (e.g., Fe-Mn oxide) phases (Boyle, 1981; Shen and Boyle, 1988; Pichat et al., 2003; Andersen et al., 2011; Hendry and Andersen, 2013). Zinc isotopes have previously been applied in Pleistocene to ancient marine sediments, typically using bulk carbonate leachates in an attempt to sidestep the contamination problem (Pichat et al., 2003; Kunzmann et al., 2013; John et al., 2017; Liu et al., 2017; Sweere et al., 2018). We propose that cold-water coral skeletons provide an exciting new possibility for a seawater Zn and Cu isotope archive. Their global distribution, combined with an ability to obtain precise ages for individual

specimens, gives corals distinct advantages over more traditional palaeoclimate archives (e.g., Robinson et al., 2014), potentially enabling reconstructions of ocean chemistry on centennial or even shorter time-scales (e.g., Wilson et al., 2014; Chen et al., 2015). In addition, their large size confers a particular advantage for analysing trace metal isotopes, because it should enable rigorous cleaning to remove surficial contaminant phases, while still providing sufficient quantities of Zn and Cu for isotope analysis.

Zinc has a classic nutrient-type distribution in the modern ocean, reflecting a combination of biological cycling and the physical ocean circulation (Bruland, 1980; Vance et al., 2017; Middag et al., 2019). Away from local sedimentary sources and hydrothermal vents, the deep ocean is isotopically homogeneous, at about $+0.45\text{‰}$ ($\delta^{66}\text{Zn}$ relative to JMC-Lyon), while the upper ocean exhibits considerable variability, ranging from -1.1 to $+1.2\text{‰}$ (Conway and John, 2014; Zhao et al., 2014; Samanta et al., 2017; John et al., 2018; Wang et al., 2018; Vance et al., 2019; Liao et al., 2020; Sieber et al., 2020). The origin of this

* Corresponding author at: Department of Earth Sciences, University College London, Gower Place, London WC1E 6BS, UK.

E-mail address: susan.little@ucl.ac.uk (S.H. Little).<https://doi.org/10.1016/j.chemgeo.2021.120304>

Received 30 November 2020; Received in revised form 23 April 2021; Accepted 2 May 2021

Available online 5 May 2021

0009-2541/© 2021 The Authors. Published by Elsevier B.V. This is an open access article under the CC BY license (<http://creativecommons.org/licenses/by/4.0/>).

variability remains a subject of debate. Biological uptake in the Southern Ocean is associated with no isotopic fractionation or with small deviations towards isotopically heavy Zn in the residual dissolved phase (Zhao et al., 2014; Wang et al., 2018; Sieber et al., 2020), consistent with evidence for limited isotopic fractionation on uptake by diatoms (John et al., 2007; Köbberich and Vance, 2017). However, marked deviations towards isotopically light sub-surface Zn are observed in the water column elsewhere (e.g., Conway and John, 2014). Explanations proposed for this phenomenon include shallow remineralisation of isotopically light organic matter (Samanta et al., 2017; Vance et al., 2019), removal by scavenging of isotopically heavy Zn (Conway and John, 2014; John and Conway, 2014; Weber et al., 2018; Liao et al., 2020), and/or inputs from an isotopically light external Zn source (Lemaitre et al., 2020; Liao et al., 2020).

Dissolved Cu concentrations in the ocean increase approximately linearly with depth (Boyle et al., 1977; Bruland, 1980). This profile shape has been described as “hybrid-type” and attributed to a combination of biological uptake and scavenging (Bruland et al., 2013). However, the respective roles of (a) reversible scavenging in the water column and (b) irreversible scavenging followed by benthic sedimentary input remain to be fully deconvolved (Boyle et al., 1977; Little et al., 2013, 2018; Roshan and Wu, 2015; Richon and Tagliabue, 2019). A key feature of Cu (and, to a lesser extent, Zn) biogeochemistry is its near ubiquitous complexation by strong organic ligands; in the ocean >99% of dissolved Cu is organically complexed (e.g., Coale and Bruland, 1988; Moffett and Dupont, 2007; Bruland et al., 2013). The isotopic composition of Cu in seawater is more sparsely documented than that of Zn. Existing data also point to a homogeneous deep ocean, at about +0.66‰ ($\delta^{65}\text{Cu}$ relative to NIST SRM 976), with deviations towards lighter Cu isotope compositions (of about +0.30‰) in the surface ocean and along some continental margins, which appear to be associated with particulate Cu input (Takano et al., 2014; Thompson and Ellwood, 2014; Little et al., 2018; Baconnais et al., 2019).

Cold water corals grow at shallow to lower bathyal water depths (bathyal zone: 1000–4000 m), and occasionally in deeper waters (Roberts et al., 2009), and therefore offer potential as an archive of intermediate and deep ocean $\delta^{66}\text{Zn}$ and $\delta^{65}\text{Cu}$ values. While the upper water column cycling of Zn and Cu isotopes is complex and incompletely understood, the relative homogeneity of modern intermediate and deep ocean Zn (and presumably, albeit to a lesser extent, Cu) isotope compositions reflects the first-order role of water masses originating from the Southern Ocean in setting global oceanic nutrient distributions (Sarmiento et al., 2004; Vance et al., 2017; de Souza et al., 2018; Sieber et al., 2020). Today, the absence of significant biological Zn isotope fractionation in the surface Southern Ocean (Zhao et al., 2014; Wang et al., 2018; Sieber et al., 2020) leads to the formation and advection northwards of intermediate (i. e. Sub-Antarctic Mode Water, SAMW, and Antarctic Intermediate Water, AAIW) and deep (Antarctic Bottom Water, AABW) water masses with the same (or very similar) isotopic compositions (Sieber et al., 2020). However, the physical, biogeochemical, and ecological characteristics of the Southern Ocean have changed through time (Sigman et al., 2010). For example, alleviation of Fe limitation in the past may have dramatically affected the nutrient status (and isotopic composition) of glacial analogues of AAIW and SAMW, as proposed for Si (e.g., Brzezinski et al., 2002; Matsumoto et al., 2002). Therefore, intermediate and deep-water Zn and Cu isotope compositions archived in cold-water corals could be used to trace past changes in biological utilization in the Southern Ocean, with implications for the global ocean carbon cycle.

In this study we evaluate the potential of cold-water corals as archives of seawater Zn and Cu isotopes. We present a series of physical and chemical cleaning experiments, followed by $\delta^{66}\text{Zn}$, $\delta^{65}\text{Cu}$, and trace element data for a suite of modern and late Holocene (<1500 yr old) cold-water corals from six oceanic regions spanning the North Atlantic to the Tasman Sea. Coral aragonite $\delta^{65}\text{Cu}$ values are distributed around the modern deep ocean Cu isotope composition, but exhibit significant

scatter. The outlook for Zn is more promising, with reasonable agreement between coral aragonite $\delta^{66}\text{Zn}$ values and measured or best estimate modern seawater $\delta^{66}\text{Zn}$ values. A small number of older fossil specimens, dated to the last glacial period, were also analysed. These corals have Zn and Cu isotope compositions similar to modern seawater values, hinting at the relative constancy of oceanic Zn and Cu cycling on glacial-interglacial timescales.

2. Samples and analytical methods

2.1. Samples

The term cold-water coral (or alternatively deep-water coral) is used here to refer to azooxanthellate scleractinian corals, of which ~90% live in deep or cold water (Roberts et al., 2009). Specimens in this study are solitary aragonitic corals of the species *Desmophyllum dianthus* and genera *Caryophyllia* and *Dasmomilia*. Taxonomic classification of samples was carried out in previous studies (listed below). *Caryophyllia* is the most diverse genus of cold-water corals, consisting of at least 66 species (Kitahara et al., 2010a). Genetic studies have highlighted the similarity of extant *Caryophyllia* and *Dasmomilia* genera (Kitahara et al., 2010b).

Two *D. dianthus* specimens of glacial age, with well-developed black or brown surface coatings (due to the presence of Fe-Mn oxide phases), were selected for cleaning experiments (described in Section 2.2). Twenty modern or late Holocene (<1500 yr old) coral specimens were then sampled, cleaned following the finalised cleaning procedure (Section 2.2), and analysed for trace element concentrations and Zn and Cu isotopes (Table 1A). Finally, four corals dated to the last glacial period (including the two specimens used in cleaning experiments) were sampled and analysed for trace element concentrations and Zn and Cu isotopes (Table 1B).

Coral samples from water depths of 170–2260 m were selected from the following locations (Fig. 1; Table 1): south of Iceland (Reykjanes Ridge), the northwest Atlantic (Manning and Muir Seamount), the eastern equatorial Atlantic (Carter Seamount), the Drake Passage (Burdwood Bank and Sars Seamount), the southwest Indian Ocean (SWIO: Coral Seamount, Melville Bank, Atlantis Bank), and south of Tasmania (South Hills and St Helens seamounts). The corals selected from these collections have previously been described and dated by uranium-series or radiocarbon in: Burke (2012), Robinson et al. (2007), Chen et al. (2016), Margolin et al. (2014), Pratt et al. (2019), and Thiagarajan et al. (2013).

2.2. Cleaning experiments

Fossil cold-water corals are often coated with a black-brown crust, made up of a mixture of iron and manganese oxides, incorporated detrital aluminosilicate grains, and occasional metal sulphides (Cheng et al., 2000). All these potential contaminating phases contain trace metals like Zn and Cu in concentrations that are orders of magnitude higher than those in coral aragonite (e.g., Boyle, 1981; Shen and Boyle, 1988). We tested the effectiveness of the physical and chemical cleaning procedures developed previously for cold-water corals (Shen and Boyle, 1988; Lomitschka and Mangini, 1999; Cheng et al., 2000; van de Fliedert et al., 2010; Crocket et al., 2014) for the analysis of Zn and Cu isotopes.

Two *D. dianthus* corals with a well-developed coating were selected for the cleaning experiments: DH115-DC-01 from the Drake Passage, and SS0108 from Tasmania (Table 1B). The black coatings of the two specimens were collected using a scalpel (coating samples were designated ‘Coat’). Thereafter, 100–150 mg coral sub-samples were obtained using a Dremel tool and progressively subjected to increasingly rigorous cleaning steps (Fig. 2):

- First, sub-samples of ‘uncleaned’ coral (designated ‘UNCL’) were rinsed three times in DI water, where rinsing refers to ultrasonication

Table 1

Location, taxonomic classification, water depth and water mass, and age of cold-water coral specimens included in this study.

A: Holocene age coral specimens

Study ID	Locality	Full ID	Genus	species	Depth (m)	Age (yr)	Modern water mass	Latitude (°N)	Longitude (°E)
Iceland									
1	Reykjanes Ridge	CE0806 D19A #2	<i>Desmophyllum</i>	<i>dianthus</i>	1545	Modern	ISOW/LSW	58.8	-32.0
2	Reykjanes Ridge	CE0806 D19A #1B	<i>Desmophyllum</i>	<i>dianthus</i>	1545	Modern	ISOW/LSW	58.8	-32.0
2 Coat	Iceland - Reykjanes Ridge	CE0806 D19A #1B	coating						
Drake Passage									
3	Burdwood Bank	NBP0805 TB04 "Big Beauty"	<i>Desmophyllum</i>	<i>dianthus</i>	816	468	AAIW	-54.4	-62.1
4	Burdwood Bank	NBP1103 DH14 Cn7	<i>Caryophyllia</i>	<i>sp.</i>	727	1170	SAMW	-54.7	-62.2
5	Sars Seamount	NBP1103 DH95 Dc7	<i>Desmophyllum</i>	<i>dianthus</i>	776	434	UCDW	-59.7	-68.9
5 Coat	Sars Seamount	NBP1103 DH95 Dc7	uncleaned coral						
6	Sars Seamount	NBP1103 DH97 Dp1	<i>Desmophyllum</i>	<i>dianthus</i>	658	281	UCDW	-59.7	-68.9
7	Sars Seamount	NBP1103 DH97 CC1	<i>Caryophyllia</i>	<i>sp.</i>	658	346	UCDW	-59.7	-68.9
7 Coat	Sars Seamount	NBP1103 DH97 CC1	coating						
Eastern Equatorial Atlantic									
8	Carter Seamount	JC094 BO244 Carls 001	<i>Caryophyllia</i>	<i>sp.</i>	621	Modern	AAIW	9.2	-21.3
9	Carter Seamount	JC094 BO712 Carlm 001	<i>Caryophyllia</i>	<i>sp.</i>	2260	Modern	NADW	9.2	-21.3
10	Carter Seamount	JC094 BO424 Das ls/m 002	<i>Dasmosmilia</i>	<i>sp.</i>	265	Modern	STMW	9.2	-21.3
11	Carter Seamount	JC094 BO457 Daslm 001	<i>Dasmosmilia</i>	<i>sp.</i>	321	Modern	STMW	9.2	-21.3
Southwest Indian Ocean									
13	Melville Bank	JC066-3245	<i>Caryophyllia</i>	<i>profunda</i>	171.9	841	STSW	-38.5	48.7
15	Coral Seamount	JC066-117	<i>Desmophyllum</i>	<i>dianthus</i>	1207.2	1476	UCDW	-41.3	42.9
15 Coat	Coral Seamount	JC066-117	coating						
14	Atlantis Bank	JC066-3697	<i>Caryophyllia</i>	<i>diomedea</i>	823	200	SAMW	-32.7	57.3
16	Atlantis Bank	JC066-3718	<i>Desmophyllum</i>	<i>dianthus</i>	1035	166	AAIW	-32.7	57.2
22	Atlantis Bank	JC066-3661	<i>Caryophyllia</i>	<i>laevigata</i>	743	762	SAMW	-32.7	57.2
23	Atlantis Bank	JC066-3705	<i>Caryophyllia</i>	<i>diomedea</i>	870	965	SAMW	-32.7	57.2
Northwest Atlantic									
17	Manning Seamount	ALV-3883-1248-003-003	<i>Desmophyllum</i>	<i>dianthus</i>	1524	118	NADW	38.2	-60.5
Tasman Sea									
19	Tasmania (S Hills - Shelf)	TN228-J2-387-1225-1253-11-1898-003	<i>Desmophyllum</i>	<i>dianthus</i>	1898	113	UCDW	-44.4	147.3
21	Tasmania (E of St Helens - East)	TN228-J2-389-0101-0930-07-1296-001	<i>Desmophyllum</i>	<i>dianthus</i>	1296	521	UCDW	-41.5	148.5

B. Glacial age coral specimens

Study ID	Locality	Full ID	Genus	species	Depth (m)	Age (yr)	Modern water mass	Latitude (°N)	Longitude (°E)
18	NW Atlantic, Muir Seamount	ALV-3885-1325-002-034	<i>Desmophyllum</i>	<i>dianthus</i>	1986	48939	NADW	33.8	-62.5
18 Coat	NW Atlantic, Muir Seamount	ALV-3885-1325-002-034	coating						
20	Carter Seamount	JC094-F00001-Desem-008	<i>Desmophyllum</i>	<i>dianthus</i>	1080	14580	AAIW/NADW	9.2	-21.3
20 Coat	Carter Seamount	JC094-F00001-Desem-008	coating						
DC-01	Sars Seamount	NBP1103 DH115 DC-01	<i>Desmophyllum</i>	<i>dianthus</i>	843	28184	UCDW	-59.7	-68.9
DC Coat	Sars Seamount	NBP1103 DH115 DC-01	coating						
SS0108	Tasmania	SS0108	<i>Desmophyllum</i>	<i>dianthus</i>	1200	73510	UCDW	-44.1	147.1
SS Coat	Tasmania	SS0108	coating						

References:

- Burke (2012): Iceland: ^{14}C .
 Margolin et al. (2014): Drake Passage: U-series.
 Chen et al. (2016): Equatorial Atlantic: U-series.
 Pratt et al. (2019): Southwest Indian Ocean: U-series.
 Robinson et al. (2007): Northwest Atlantic: U-series.
 Thiagarajan et al. (2013): Tasman Sea: ^{14}C .
 DC and SS: Cleaning specimens; see Table 2.
Lat/Long in italics: approximate location.

of the coral fragments in DI water in acid-cleaned 15 mL centrifuge tubes for 60 s, followed by removal of the supernatant by pipette.

- Second, three to four sub-samples were carefully physically cleaned using a Dremel tool and rinsed three times in DI water (designated 'PHYS'). During physical cleaning, any coatings were removed, as well as epibiont boreholes and other discoloration or impurities within the skeleton, including remineralised or secondary calcium carbonate.
- Third, three to four sub-samples were subject to physical cleaning and an oxidising chemical 'pre-cleaning' procedure (designated 'OXIC'). The chemical pre-cleaning procedure consisted of ultrasonication in a series of oxidative cleaning solutions, targeting residual organic phases (Shen and Boyle, 1988), with rinses in DI water (for details, see Fig. 2).
- Finally, three to four sub-samples were subjected to the full physical and chemical cleaning procedure described by van de Flierdt et al. (2010) and detailed in Fig. 2 (designated 'FULL'). The major difference between the pre-cleaning and full chemical cleaning procedures is the addition of a reductive cleaning step, which aims to remove trace metals associated with residual iron and manganese oxides (van de Flierdt et al., 2010).

For all other coral specimens for which data are reported in this study, sub-samples of 80–200 mg were subjected to the full physical and chemical cleaning procedure (Fig. 2). Chemical cleaning led to an average mass loss of $7.0 \pm 3.5\%$ (1SD, $n = 36$, range 1.9–21%). Where possible, samples were analysed for Zn and Cu isotope compositions in duplicate (i. e. two coral sub-samples were separately cleaned, digested, and analysed). Four of the Holocene corals and all four glacial-age coral specimens had well-developed coatings (Table 1), which were also analysed to evaluate the possibility of residual contamination by Fe–Mn oxide or detrital (aluminosilicate) phases.

2.3. Analytical procedures

Sample digestion and column chemistry was carried out in the MAGIC clean laboratories at Imperial College London. Throughout, deionized 18.2 M Ω water (MQ), Teflon-distilled acids (HNO₃ and HCl), Suprapur H₂O₂, and acid-cleaned Savillex PFA labware were used. In preparation for analysis, corals and coatings were carefully bulk digested in 1 mL 6 M HCl (carbonate effervesces vigorously on addition of acid). For coral samples with significant coatings, residual contamination was assessed using a mass balance approach and found to be negligible (see Section 4.2, Table S3). Samples were then dried and redissolved in 5 mL 1 M HCl.

An aliquot of this coral digest solution was diluted in 2% HNO₃ to give approximately 100 ppb Ca concentrations for multi-element analysis on a Thermo Element XR at ETH Zürich. The elements Li, Na, Mg, Al, Mn, Fe, Cu, Zn, Sr, Cd, Ba, and U were measured as metal/Ca ratios following the procedure outlined in Hasenfratz et al. (2017). Accuracy and precision of the instrument were assessed by routine measurements of four consistency standards (Table S1), of which three are gravimetrically prepared in-house standards (CS1, CS2, CS3) and one is a carbonate rock standard purchased from LGC Standards (NCS DC70303).

The appropriate volume of a ^{64}Zn - ^{67}Zn double spike was added to all samples to achieve a spike:sample ratio of approximately 1.2 (Arnold et al., 2010; Bridgestock et al., 2014). In order to obtain ≥ 40 ng Zn for isotope analysis, some sub-samples from the cleaning experiments were combined (Table 2). The Zn and Cu fractions were then purified using a two-step column chromatography procedure using AG MP-1 M resin (BioRad), as detailed previously (Maréchal et al., 1999; Archer and Vance, 2004; Little et al., 2014). The second Zn column was smaller in volume, following Bridgestock et al. (2014). Prior to analysis, purified Zn and Cu fractions were oxidised by treatment with $2 \times \sim 100 \mu\text{L}$ 14 M HNO₃ (Zn) or refluxing overnight with 14 M HNO₃ + H₂O₂ (Cu), before final dissolution in 2% HNO₃. Procedural Zn and Cu blanks were < 1 ng.

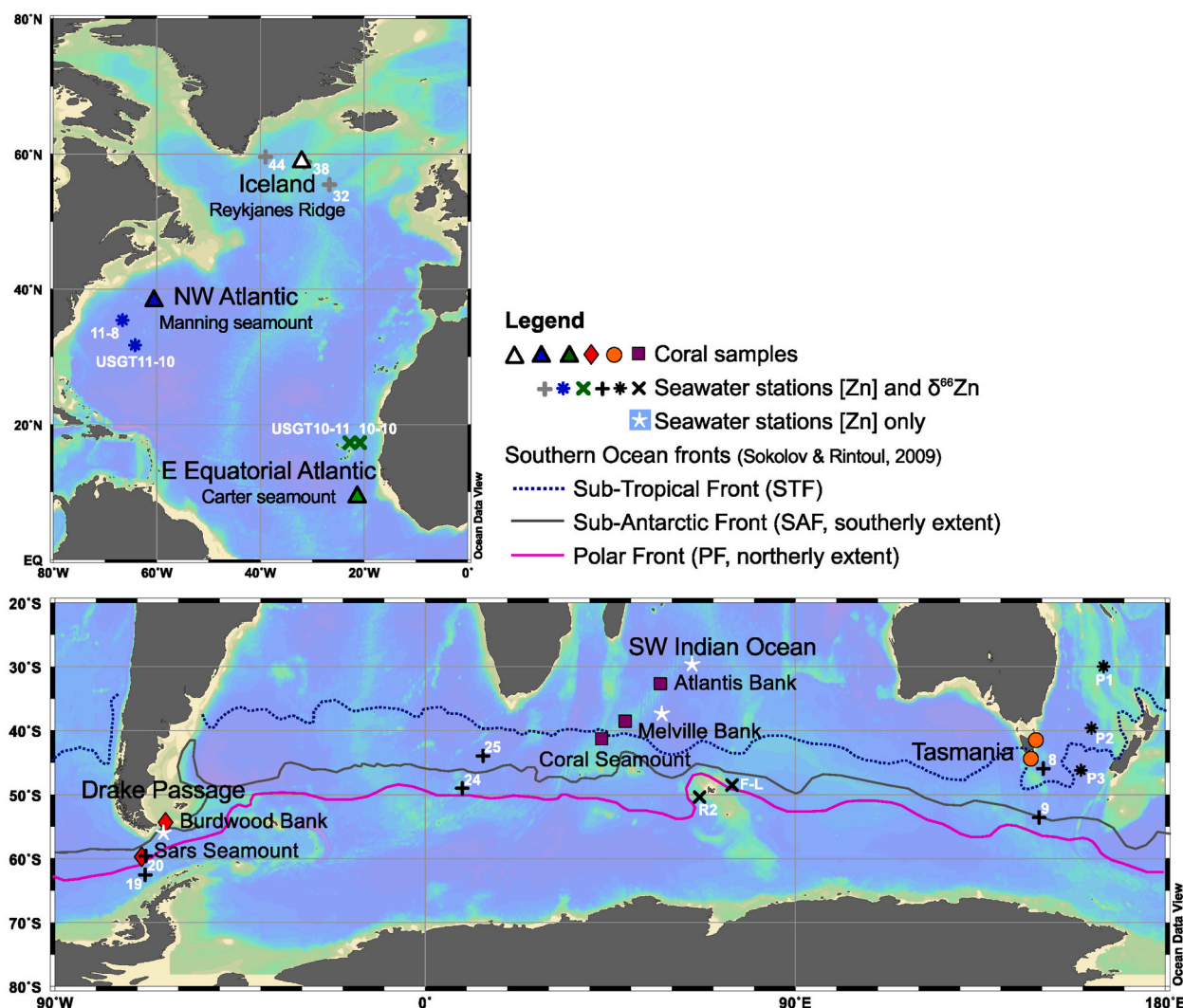


Fig. 1. Maps showing the locations of Holocene coral specimens (filled symbols) and their nearest or most closely equivalent seawater sampling locations (* × + ☆). Locations of the major Southern Ocean fronts are also shown (after Sokolov and Rintoul, 2009). Proximal seawater stations with published Zn isotope compositions as follows: Iceland, grey + (Lemaitre et al., 2020); North Atlantic, blue * and green × (Conway and John, 2014); Southern Ocean, black + (Sieber et al., 2020), black × (Wang et al., 2018); Tasman Sea, black * (Samanta et al., 2017). Seawater stations with Zn concentrations only (white ☆) from GEOTRACES IDP 2017 (Schlitzer et al., 2018). Station numbers are in white text.

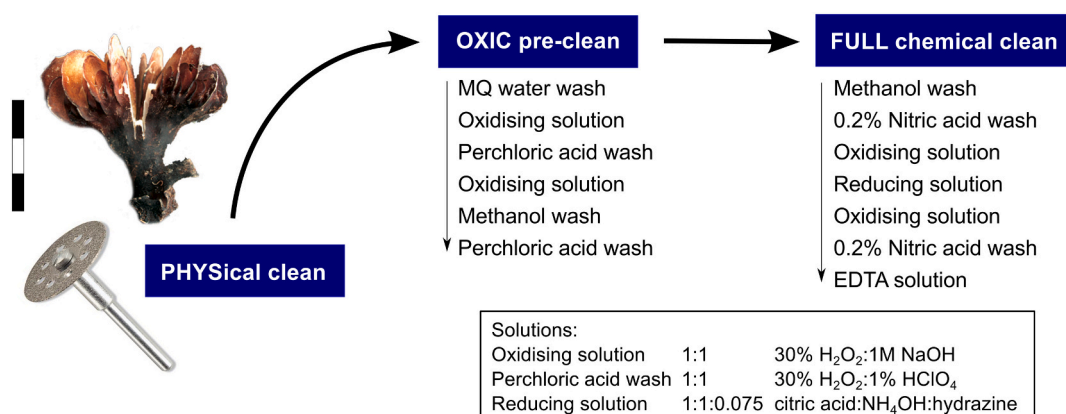


Fig. 2. Schematic illustration of the protocol for progressive cleaning of coral samples, based on van de Flierdt et al. (2010).

Table 2

Cleaning experiment results for two *D. dianthus* corals with well-developed coatings: DH115-DC-01 from the Drake Passage, and SS0108 from Tasmania. Trace element/Ca ratios (from ICP-MS, except Zn^a), Zn and Cu concentrations and isotope compositions.

Sample ID	Li/Ca μmol/mol	Na/Ca mmol/mol	Mg/Ca mmol/mol	Al/Ca μmol/mol	Mn/Ca μmol/mol	Fe/Ca μmol/mol	Cu/Ca μmol/mol	Zn/Ca ^s μmol/mol	Sr/Ca mmol/mol	Cd/Ca μmol/mol	Ba/Ca μmol/mol	U/Ca nmol/mol	Zn ^s μg/g	δ ⁶⁶ Zn ‰	2SE	Cu μg/g	δ ⁶⁵ Cu ‰	2SE
DH115-DC-01, Drake Passage																		
DC-Coat	18.6	39.5	7.68	2646	13840	20206	51.6	244.5	sat	0.94	142.7	3544	146.1	0.55	0.05	60.30	-0.01	0.04
UNCL	12.1	17.0	1.78	156	496	868	6.27	3.26	sat	0.50	26.1	2686	3.26	0.70	0.05	3.41	0.13	0.04
PHYS-1	9.6	17.8	1.69	bd	0.38	2.38	0.51	0.90	sat	0.58	14.0	2607	0.90	0.46	0.05	0.33		
PHYS-2	9.6	17.4	1.60	bd	0.34	1.67	0.45	0.37	sat	0.55	14.8	2862	0.37	0.40	0.05	0.28	0.78	0.04
PHYS-3	9.8	17.4	1.64	bd	0.22	1.30	0.44	0.58	sat	0.54	14.2	2686	0.58	0.46	0.07	0.33		
PHYS-4	9.0	17.5	1.62	bd	1.00	1.55	0.80	0.42	13.2	0.60	15.2	2938	0.42	0.41	0.04	0.46	0.85	0.04
OXIC-1	10.0	17.5	1.60	bd	0.71	2.83	0.74	0.38	sat	0.55	14.2	2753	0.38	0.46	0.04	0.48	0.68	0.05
OXIC-2	11.3	18.0	1.79	bd	0.25	3.23	0.49	0.84	sat	0.57	14.1	2561	0.84	0.36	0.03	0.32		
OXIC-3	10.8	17.5	1.57	bd	0.56	2.20	0.58	0.37	sat	0.56	15.2	3025	0.37	0.44	0.04	0.36		
OXIC-4	9.1	17.4	1.57	bd	0.45	1.92	0.52	0.48	13.4	0.59	15.2	3059	0.48	0.40	0.03	0.29	0.89	0.03
FULL-1	8.7	17.0	1.54	bd	0.12	0.66	0.38	0.68	sat	0.56	14.3	2717	0.68	0.39	0.04	0.25		
FULL-2	9.1	17.1	1.50	bd	0.07	1.01	0.37	0.43	sat	0.53	13.9	2890	0.43	0.36	0.04	0.22		
FULL-3	10.8	17.9	1.75	2.2	1.23	5.18	0.67	0.57	sat	0.57	14.3	2624	0.57	0.40	0.04	0.34	0.84	0.04
FULL-4	9.0	17.7	1.61	bd	0.12	1.06	0.48	0.38	13.0	0.59	14.6	2950	0.38	0.39	0.03	0.27	0.85	0.05
SS0108, Tasmania																		
SS-Coat	24.4	43.7	9.93	2457	1805	3640	20.6	28.5	11.9	1.15	65.6	2430	18.6	0.25	0.05	8.22	0.23	0.02
UNCL-1	11.1	17.3	1.94	358	64	272	2.94	1.94	12.7	0.94	16.4	2086	1.27	0.26	0.06	0.93	0.38	0.03
UNCL-2	10.7	17.0	2.00	247	30	164	2.52	1.35	12.5	0.95	15.2	2162	0.88	0.22	0.05	1.60	0.30	0.03
UNCL-3	11.9	17.4	1.99	441	51	344	4.25	2.49	12.8	1.03	17.5	2220	1.63	0.22	0.03	1.35	0.34	0.04
PHYS-1	9.6	17.3	1.88	24	0.89	20.0	1.44		12.8	0.99	14.4	1977						
PHYS-3	9.8	17.6	1.93	34	1.43	21.9	1.63	0.62	12.6	1.02	14.5	1978	0.44	0.38	0.06	0.97	0.51	0.03
PHYS-2	10.2	17.4	1.88	33	4.64	22.4	1.85	0.62	12.6	1.03	14.3	1984	0.32	0.27	0.05	1.18	0.39	0.02
OXIC-1	9.7	17.7	1.90	16	0.90	10.7	1.36	0.50	12.3	0.98	14.0	1881	0.33	-		0.86	0.54	0.02
OXIC-2	11.7	18.6	2.23	38	1.51	44.6	2.96		12.8	1.06	15.7	1883						
OXIC-3	10.0	17.8	1.86	42	0.99	30.1	1.90	0.71	12.5	1.04	14.5	2001	0.46	0.39	0.04	1.56	0.43	0.03
OXIC-4	10.6	17.6	1.98	13	0.62	12.3	1.24	0.48	sat	0.99	13.9	1831	0.31	0.45	0.05	0.79	0.46	0.05
FULL-1	9.6	18.1	1.85	18	0.42	14.4	0.61		12.4	1.03	13.9	1834						
FULL-2	9.5	18.0	1.85	15	0.44	9.4	0.58	0.50	12.5	1.03	14.1	1933	0.33	0.40	0.04	0.35	0.75	0.03
FULL-3	10.0	17.9	1.80	19	0.31	13.5	0.44		12.4	1.04	14.2	1822						
FULL-4	10.4	18.0	1.93	13	0.31	15.7	0.58	0.51	Sat	0.98	13.6	1828	0.33	0.34	0.05	0.39		

See main text for description of sample ID codes (Coat, UNCL, PHYS, OXIC, FULL).

bd: Al concentrations below detection limit, where detection limit estimated at 3 × blank.

sat: >10⁹ counts Sr during Element analysis.

^aZn concentrations calculated by isotope dilution (Ca concentration for Zn/Ca calculated based on coral mass and molecular mass of CaCO₃). N.B. Excludes Zn/Ca ratios of coatings, which are from Element ICP-MS.

Merged aliquots for isotope analysis on Tasmania coral (SS0108) samples: PHYS-1 and PHYS-3; OXIC-2 and OXIC-3; FULL-1, FULL-2, and FULL-3.

External 2SD on δ⁶⁶Zn = 0.07‰, and on δ⁶⁵Cu = 0.11‰ (based on repeat analyses of secondary carbonate standard).

Table 3

Trace element/Ca ratios of cold-water corals.

A: Holocene age coral specimens

Sample ID ^a	Locality	Species	Depth (m)	Age (yr)	Li/Ca μmol/mol	Na/Ca mmol/mol	Mg/Ca mmol/mol	Al/Ca μmol/mol	Mn/Ca μmol/mol	Fe/Ca μmol/mol	Cu/Ca μmol/mol	Zn/Ca ^b μmol/mol	Sr/Ca mmol/mol	Cd/Ca μmol/mol	Ba/Ca μmol/mol	U/Ca nmol/mol
Iceland																
1A	Reykjanes Ridge	<i>D. dianthus</i>	1545	Modern	15.0	23.2	3.63	bd	0.15	0.83	0.38	0.42	13.1	0.06	8.0	1166
1B					13.7	22.5	3.37	bd	0.06	1.25	0.29	-	12.5	0.05	7.5	1189
1C					14.9	23.4	3.70	bd	0.28	0.91	0.47	0.77	12.5	0.06	7.7	1117
2A	Reykjanes Ridge	<i>D. dianthus</i>	1545	Modern	13.3	22.5	3.42	bd	0.23	0.90	0.45	2.90	12.6	0.06	7.7	1193
2B					12.5	21.6	3.19	bd	0.21	0.81	0.27	3.07	12.4	0.06	7.5	1194
2 Coat	Coating				11.9	31.6	8.58	306	92	1753	19.9	54.4	12.4	0.88	9.6	1636
Drake Passage																
3A	Burdwood Bank	<i>D. dianthus</i>	816	468	8.2	18.7	2.01	bd	0.08	0.86	0.20	1.20	12.8	0.12	12.4	2218
3B					8.5	19.2	2.11	bd	0.12	1.03	0.22	1.43	12.9	0.12	12.5	2205
3C					9.4	19.1	2.23	bd	0.29	0.81	0.17	-	12.8	0.13	11.9	1993
4A	Burdwood Bank	<i>Caryophyllia</i>	727	1170	8.4	17.2	1.95	bd	0.14	0.19	0.13	0.86	12.8	0.34	12.0	1674
4B					nd	nd	nd	nd	nd							
5A	Sars Seamount	<i>D. dianthus</i>	776	434	10.5	20.0	2.62	bd	0.07	0.49	0.23	2.24	12.8	0.60	14.7	1754
5B					10.7	19.8	2.59	bd	0.04	1.03	0.18	-	13.0	0.58	14.1	1659
5D					12.7	20.7	3.12	bd	0.02	0.69	0.11	2.93	12.9	0.54	14.2	1414
5 Coat	Unclean coral				11.1	29.4	5.45	2208	109	1918	3.80	4.80	12.6	0.60	22.7	2074
6A	Sars Seamount	<i>D. dianthus</i>	658	281	10.7	20.2	2.71	bd	0.16	0.72	0.25	1.43	13.2	0.79	14.5	1840
6B					11.1	20.2	2.90	2.6	0.08	0.51	0.19	-	12.9	0.72	13.8	1734
7	Sars Seamount	<i>Caryophyllia</i>	658	346	11.7	20.7	2.77	3.1	0.26	0.32	0.47	9.33	13.1	0.17	16.2	1760
7 Coat	Coating				9.8	31.4	6.60	323	3704	2483	15.9	27.0	13.3	0.43	39.1	2464
Eastern Equatorial Atlantic																
8A	Carter Seamount	<i>Caryophyllia</i>	621	Modern	8.8	19.7	2.49	bd	0.48	3.40	0.77	12.4	12.3	1.59	10.3	1758
8B					9.8	20.2	2.73	bd	0.41	3.70	0.76	12.7	12.2	1.31	10.2	1565
9	Carter Seamount	<i>Caryophyllia</i>	2260	Modern	7.9	15.9	1.65	bd	0.16	0.25	0.13	2.99	12.3	0.37	10.3	1771
10	Carter Seamount	<i>Dasmomilia</i>	265	Modern	10.4	23.7	3.59	bd	0.25	0.35	0.34	2.18	12.4	0.15	8.0	1102
11A	Carter Seamount	<i>Dasmomilia</i>	321	Modern	10.2	22.8	3.34	bd	0.20	0.67	0.21	0.49	12.4	0.20	8.3	1256
11B					8.8	17.2	1.90	bd	0.20	0.20	0.11	-	12.7	0.37	10.1	1658
Southwest Indian Ocean																
13	Melville Bank	<i>C. profunda</i>	172	841	8.9	18.5	2.41	bd	0.47	0.26	0.32	2.15	12.9	0.73	14.2	1820
15	Coral Seamount	<i>D. dianthus</i>	1207	1476	9.8	19.5	2.13	bd	0.18	2.20	0.21	1.87	12.9	0.16	15.1	2182
15 Coat	Coating				17.1	46.4	8.07	1207	2931	2105	15.7	54.1	11.8	0.36	50.4	2037
14	Atlantis Bank	<i>C. diomedea</i>	823	200	11.3	21.8	3.31	bd	0.38	2.89	0.37	2.56	12.2	1.25	8.4	1316
16A	Atlantis Bank	<i>D. dianthus</i>	1035	166	13.4	22.5	4.32	bd	0.21	1.87	0.16	1.04	12.2	0.13	10.2	1349
16B					13.9	23.2	4.57	bd	0.16	2.50	0.15	0.84	12.5	0.12	10.3	1286
22	Atlantis Bank	<i>C. laevigata</i>	743	762	10.8	21.7	3.50	bd	0.16	1.59	0.80	5.87	12.6	0.76	7.8	1400
23	Atlantis Bank	<i>C. diomedea</i>	870	965	9.9	20.4	3.15	bd	0.06	1.21	0.78	16.8	12.2	1.91	8.6	1451
Northwest Atlantic																
17A*	Manning Seamount	<i>D. dianthus</i>	1524	118	10.8	20.3	2.59	14.7	0.13	6.68	0.16	0.52	12.0	0.08	8.3	1410
17B*					11.5	21.0	2.82	28.5	0.50	15.2	0.22	0.58	12.4	0.10	8.8	1410
Tasman Sea																
19	South Hills - Shelf	<i>D. dianthus</i>	1898	113	8.3	18.2	1.96	bd	0.07	2.47	0.31	2.24	12.0	0.43	14.8	1969
21	East of St Helens	<i>D. dianthus</i>	1296	521	11.7	20.0	3.42	1.6	0.34	1.58	1.00	2.63	12.4	0.11	15.3	1753

B: Glacial age coral specimens

Sample ID ^a	Locality	Species	Depth (m)	Age (yr)	Li/Ca $\mu\text{mol/mol}$	Na/Ca mmol/mol	Mg/Ca mmol/mol	Al/Ca $\mu\text{mol/mol}$	Mn/Ca $\mu\text{mol/mol}$	Fe/Ca $\mu\text{mol/mol}$	Cu/Ca $\mu\text{mol/mol}$	Zn/Ca ^b $\mu\text{mol/mol}$	Sr/Ca mmol/mol	Cd/Ca $\mu\text{mol/mol}$	Ba/Ca $\mu\text{mol/mol}$	U/Ca mmol/mol
18A	NW Atlantic, Muir-Seamount	<i>D. dianthus</i>	1986	48939	12.4	18.8	2.36	4.9	0.12	4.53	0.27	2.39	12.3	0.28	13.5	1445
18B	Muir-Seamount	<i>D. dianthus</i>	1986	48939	11.6	18.7	2.28	bd	0.07	2.31	0.24	3.02	12.2	0.31	13.3	1537
18 Coat		Coating			13.2	181	135	38404	367896	442651	424	1035	9.5	4.20	923	10508
20	Equat. Atlantic, Carter Seamount	<i>D. dianthus</i>	1080	14580	8.3	18.2	1.99	7.8	1.18	5.65	0.16	0.65	12.5	0.25	11.8	2011
20 Coat		Coating			46.5	27.5	9.74	10005	5422	18053	18.7	37.0	10.9	0.91	59.5	2337
SS	Tasman Sea	<i>D. dianthus</i>	1200	73510	9.9	18.0	1.86	16.1	0.37	13.3	0.55	0.50	12.4	1.02	14.0	1854
SS Coat		Coating			24.4	43.7	9.93	2457	1805	3640	20.6	28.5	11.9	1.15	65.6	2430
DC	Drake Passage, Sars Seamount	<i>D. dianthus</i>	843	28184	9.4	17.4	1.60	bd	0.38	1.98	0.47	0.52	13.0	0.56	14.3	2795
DC Coat		Coating			18.6	39.5	7.68	2646	13840	20206	51.6	244	sat	0.94	143	3544

bd: Al concentrations below detection limit, where detection limit estimated at $3 \times$ blank

^aLetters after sample numbers (A-D) indicate full replicate sub-samples

^bZn concentrations calculated by isotope dilution (Ca concentration calculated based on coral mass and molecular mass of CaCO_3). N.B. Excludes Zn/Ca ratios of coatings, which are from Element ICP-MS. All other Me/Ca ratios from ICP-MS.

^cSample 17 (particularly sub-sample 17B) remained visibly unclean after physical cleaning

Cleaned coral Zn concentrations and Zn/Ca ratios were calculated using isotope dilution (Zn/Ca_{ID} , based on data from the Nu Plasma) for comparison with Element-derived ($\text{Zn/Ca}_{\text{Element}}$) ratios. Calcium concentrations (required to calculate Zn/Ca ratios) were estimated based on the mass of the coral sub-sample and molecular mass of CaCO_3 . $\text{Zn/Ca}_{\text{Element}}$ and Zn/Ca_{ID} are typically in agreement, with $\text{Zn/Ca}_{\text{Element}} = 113 \pm 29\%$ of Zn/Ca_{ID} (1SD, $n = 33$). However, Element-derived Zn/Ca ratios approach blank levels (i. e. detection limit) at the very low Zn concentrations found in cleaned corals, hence Zn and Zn/Ca values from isotope dilution are reported in Tables 2–4.

Analytical protocols for isotopic analysis have been described previously for Cu in Little et al. (2014, 2017) and for Zn in Arnold et al. (2010), Bridgestock et al. (2014), and Little et al. (2019). Both Cu and Zn isotope ratios were blank-corrected using a prior analysis of the 2% HNO_3 solution used to dilute the samples. In brief, Cu isotope ratios were analysed in low resolution mode on a Neptune Plus MC-ICP-MS at ETH Zürich. Sample introduction was via a Savillex C-Flow PFA nebulizer (50 $\mu\text{l}/\text{min}$) attached to a glass spray chamber. Copper isotope ratios for samples were calculated using a standard bracketing approach by comparison to pure untreated NIST SRM 976 and are reported relative to this standard in delta (per mil, ‰) notation:

$$\delta^{65/63}\text{Cu} = \left(\frac{\left(\frac{^{65}\text{Cu}/^{63}\text{Cu}}{\text{SRM 976}} \right)_{\text{sample}} - 1}{\left(\frac{^{65}\text{Cu}/^{63}\text{Cu}}{\text{SRM 976}} \right)_{\text{SRM 976}}} \right) \times 1000 \quad (1)$$

Samples analysed for Cu isotope compositions on two measurement days, including the initial analysis of cleaning experiments from DH115-DC-01, the first batch of Holocene samples, and one SS0108 sub-sample (FULL-4), exhibited anomalously light Cu isotope signatures and apparently elevated Cu concentrations (as calculated from beam-matching during the isotopic analysis) compared to those measured prior to chemistry using the Element ICP-MS. These samples did not show elevated Na or Mg concentrations after chemistry, but the presence of an unidentified isobaric interference on ^{63}Cu , or contamination, is considered probable. These data are excluded from the final datasets presented in Tables 2 and 4. Copper samples from all subsequent batches of Holocene and glacial-age corals, and duplicated cleaning experiment samples for DH115-DC-01, were subject to a third Cu clean-up column and no further discernible issues were encountered.

Zinc isotope ratios were analysed in low resolution mode at Imperial College London on a Nu Plasma HR MC-ICP-MS equipped with an ARIDUS II (CETAC Technologies) desolvating system and nominal 100 $\mu\text{L}/\text{min}$ MicroMist glass nebulizer. Instrumental mass bias was corrected via a double-spike technique (Arnold et al., 2010) using the offline data-reduction procedure of Siebert et al. (2003). Interference corrections for ^{64}Ni (monitoring mass 62) and Ba^{2+} (monitoring mass 68.5) were negligible. The Zn isotope ratios of samples were determined relative to matching (spike:natural Zn ratio and total Zn) standard solutions of IRMM-3702:

$$\delta^{66/64}\text{Zn} = \left(\frac{\left(\frac{^{66}\text{Zn}/^{64}\text{Zn}}{\text{IRMM-3702}} \right)_{\text{sample}} - 1}{\left(\frac{^{66}\text{Zn}/^{64}\text{Zn}}{\text{IRMM-3702}} \right)_{\text{IRMM-3702}}} \right) \times 1000 \quad (2)$$

Final $\delta^{66}\text{Zn}$ values are reported normalised to JMC Lyon by applying a correction of $+0.30\%$, as recommended by Moynier et al. (2017).

Accuracy and reproducibility of $\delta^{66}\text{Zn}$ and $\delta^{65}\text{Cu}$ values were assessed by repeated analysis of secondary solution standards (London Zn, AM Cu), as well as digestion and analysis of several USGS rock standards (Nod P1, BCR-2, BHVO-2, BIR-1, SGR-1), and a carbonate consistency standard (NCS DC70303), and are reported in Table S2. Data for these standards agree with literature values, where available (Bigalke et al., 2010; Moynier et al., 2017). Error bars on figures are the external 2SD reproducibility of the carbonate consistency standard (NCS DC70303: $\delta^{65}\text{Cu} = 0.21 \pm 0.11\%$, $\delta^{66}\text{Zn} = 0.76 \pm 0.07\%$) or internal 2SE on individual isotope ratios, whichever is larger.

Table 4

Cold-water coral Zn/Ca and Cu/Ca ratios, calculated partition coefficients D_{Zn} and D_{Cu} , and Zn and Cu isotope compositions. Also given are estimates of ambient seawater Zn and Cu concentrations (from which coral D_{Zn} and D_{Cu} values were calculated) and $\delta^{66}Zn$ values.

A: Holocene age coral specimens

Sample ID	Locality	Species	Depth (m)	Age (yr)	Coral Zn		Ambient seawater Zn				Coral Cu		Ambient seawater Cu			
					Zn/Ca ^s μmol/mol	D_{Zn}	$\delta^{66}Zn$ ‰ ± 2SE	Estimated [Zn] nmol/kg	Ref	Estimated $\delta^{66}Zn$ ‰, 1SD (range)	Ref	Cu/Ca μmol/mol	D_{Cu}	$\delta^{65}Cu$ ‰ ± 2SE	Estimated [Cu] nmol/kg	Ref
Iceland																
1A	Reykjanes Ridge	<i>D. dianthus</i>	1545	Modern	0.42		+0.67 ± 0.05						0.38		-	
1B					-	(1.0 to) 4.4	-	1.4 (to 6.0)	a	+0.47 ± 0.06 (-0.2 to +0.5)	a	0.29	2.8	+0.45 ± 0.05	1.4 ± 0.2	IDP17
1C					0.77		+0.55 ± 0.03					0.47		+0.25 ± 0.06		
2A	Reykjanes Ridge	<i>D. dianthus</i>	1545	Modern	2.90		+0.68 ± 0.04	1.4 (to 6.0)	a	+0.47 ± 0.06 (-0.2 to +0.5)	a	0.45	3.3	+0.76 ± 0.06	1.4 ± 0.2	IDP17
2B					3.07	(5.1 to) 22	+0.64, +0.59				0.27		-			
2 Coat					Coating	54.4		+0.37 ± 0.04				19.9		+0.26 ± 0.04		
Drake Passage																
3A	Burdwood Bank, N of SAF	<i>D. dianthus</i>	816	468	1.20		+0.37 ± 0.03						0.20		-	
3B					1.43	4.4	+0.37, +0.41	3.1 ± 0.6	b	+0.42 ± 0.08	b	0.22	1.3	-	1.3 ± 0.2	f
3C					-		-					0.17		+0.32 ± 0.13		
4A	Burdwood Bank	<i>Caryophyllia</i>	727	1170	0.86	3.1	+0.36 ± 0.03	2.8 ± 0.3	b	+0.42 ± 0.08	b	0.13	1.1	-	1.2 ± 0.2	f
4B					-		-				nd		+0.55 ± 0.16			
5A	Sars Seamount, between PF and SAF	<i>D. dianthus</i>	776	434	2.24		+0.39 ± 0.03						0.23		-	
5B					-	4.5	-	5.9 ± 0.3	c	+0.39 ± 0.04	c	0.18	1.0	+0.76 ± 0.10	1.85 ± 0.1	f
5D					2.93		+0.32 ± 0.04					0.11		-		
5 Coat	Coating	Unclean coral			4.80		+0.58 ± 0.05						3.80		+0.11 ± 0.04	
6A	Sars Seamount	<i>D. dianthus</i>	658	281	1.43		+0.33, +0.35						0.25		-	
6B					-	2.6	-	5.7 ± 0.3	c	+0.39 ± 0.04	c	0.19	1.1	+0.85 ± 0.10	1.8 ± 0.1	f
7					<i>Caryophyllia</i>	658	346	9.33	17	+0.44 ± 0.04	5.7 ± 0.3	c	+0.39 ± 0.04	c	0.47	2.7
7 Coat	Coating				27.0		+0.61 ± 0.04						15.9		+0.18 ± 0.05	
Eastern Equatorial Atlantic																
8A	Carter Seamount	<i>Caryophyllia</i>	621	Modern	12.4	92	+0.35 ± 0.04	1.4 ± 0.2	d	+0.33 ± 0.14	d	0.77	7.2	-	1.1 ± 0.1	g
8B					12.7		+0.30, +0.33					0.76		-		
9	Carter Seamount	<i>Caryophyllia</i>	2260	Modern	2.99	18	+0.63 ± 0.03	1.7 ± 0.2	d	+0.59 ± 0.04	d	0.13	0.9	-	1.5 ± 0.1	g
10	Carter Seamount	<i>Dasmomilia</i>	265	Modern	2.18	45	+0.64 ± 0.04	0.5 ± 0.2	d	+0.18 ± 0.18	d	0.34	3.8	-	0.9 ± 0.1	g
11A	Carter Seamount	<i>Dasmomilia</i>	321	Modern	0.49	8.4	+0.57 ± 0.04	0.6 ± 0.2	d	+0.42 ± 0.08	d	0.21	1.2	-	0.9 ± 0.1	g
11B					-		-					0.11		+0.95 ± 0.12		
Southwest Indian Ocean																
13	Melville Bank	<i>C. profunda</i>	171.9	841	2.15	25	+0.60 ± 0.04	0.9 ± 0.2	IDP17	+0.4 ± 0.2	x	0.32	4.6	+0.27 ± 0.05	0.7 ± 0.2	IDP17
15	Coral Seamount	<i>D. dianthus</i>	1207.2	1476	1.87	5.1	+0.58 ± 0.03	3.8 ± 0.6	IDP17	+0.42 ± 0.08	b	0.21	2.4	+0.44 ± 0.05	0.9 ± 0.1	IDP17
15 Coat	Coating				54.1		+0.60 ± 0.03						15.7		+0.26 ± 0.05	
14	Atlantis Bank	<i>C. diomedea</i>	823	200	2.56	18	+0.07 ± 0.03	1.5 ± 0.3	IDP17	+0.42 ± 0.08	b	0.37	4.4	+0.50 ± 0.05	0.85 ± 0.1	IDP17
16A	Atlantis Bank	<i>D. dianthus</i>	1035	166	1.04		+0.39 ± 0.04						0.16		+0.59 ± 0.07	
16B					0.84	4.0	+0.48 ± 0.03	2.4 ± 0.3	IDP17	+0.42 ± 0.08	b	0.15	1.7	+0.68 ± 0.09	0.95 ± 0.1	IDP17
22	Atlantis Bank	<i>C. laevigata</i>	743	762	5.87	43	+0.29 ± 0.04	1.4 ± 0.3	IDP17	+0.42 ± 0.08	b	0.80	10.3	+0.59 ± 0.05	0.8 ± 0.1	IDP17
23	Atlantis Bank	<i>C. diomedea</i>	870	965	16.8	91	+0.39 ± 0.04	1.9 ± 0.3	IDP17	+0.42 ± 0.08	b	0.78	8.9	+1.05 ± 0.09	0.9 ± 0.1	IDP17
Northwest Atlantic																
17A*	Manning Seamount	<i>D. dianthus</i>	1524	118	0.52	3.8	0.61 0.04	1.5 ± 0.2	d	+0.46 ± 0.04	d	0.16	1.2	0.62 0.07	1.35 ± 0.1	g
17B*					0.58		0.54 0.04					0.22		0.54 0.04		
Tasman Sea																
19	South Hills - Shelf	<i>D. dianthus</i>	1898	113	2.24	4.4	+0.29 ± 0.04	5.3 ± 0.3	e	+0.48 ± 0.05	e	0.31	1.6	+0.54 ± 0.04	2.0 ± 0.1	h
21	East of St Helens	<i>D. dianthus</i>	1296	521	2.63	6.5	+0.48 ± 0.03	4.2 ± 0.6	e	+0.51 ± 0.07	e	1.00	6.4	+0.30 ± 0.05	1.6 ± 0.1	h

B: Glacial age coral specimens

Sample ID	Locality	Species	Depth (m)	Age (yr)	Coral Zn		Coral Cu	
					Zn/Ca ^s μmol/mol	δ ⁶⁶ Zn ‰ ± 2SE	Cu/Ca μmol/mol	δ ⁶⁵ Cu ‰ ± 2SE
18A	NW Atlantic, Muir Seamount	<i>D. dianthus</i>	1986	48939	2.39	+0.66 ± 0.03	0.27	+0.69 ± 0.05
18B					3.02	+0.68 ± 0.03	0.24	+0.62 ± 0.06
18 Coat		Coating			1035	+0.90 ± 0.03	424	0.00 ± 0.03
20	Carter Seamount	<i>D. dianthus</i>	1080	14580	0.65	+0.79 ± 0.04	0.16	+0.70 ± 0.07
20 Coat					37.0	+0.51 ± 0.04	19	+0.22 ± 0.04
SS	Tasman Sea	<i>D. dianthus</i>	1200	73510	0.50	+0.37 ± 0.04	0.55	+0.73 ± 0.04
SS Coat					28.5	+0.25 ± 0.05	20.6	+0.23 ± 0.02
DC	Sars Seamount	<i>D. dianthus</i>	843	28184	0.52	+0.38 ± 0.04	0.47	+0.84 ± 0.02
DC Coat					244	+0.55 ± 0.05	51.6	-0.01 ± 0.04

^sZn concentrations calculated by isotope dilution (Ca concentration calculated based on coral mass and molecular mass of CaCO₃). N.B. Excludes Zn/Ca ratios of coatings, which are from Element ICP-MS. All other Me/Ca ratios from ICP-MS.

Two Zn isotope values for the same sub-sample indicate reanalysis of the sub-sample after a third Zn clean-up column.

*Sample 17 (particularly sub-sample 17B) remained visibly unclean after physical cleaning.

#Partition coefficients were calculated as per equations (3) and (4). For corals analysed in duplicate or triplicate, the mean of measured coral Zn/Ca and Cu/Ca values were used.

External 2SD on δ⁶⁶Zn = 0.07‰, and on δ⁶⁵Cu = 0.11‰ (based on repeat analyses of secondary carbonate standard).

Error bars on figures are the external 2SD, except where the internal 2SE is larger (for samples with low Cu contents).

References:

a. [Lemaitre et al. \(2020\)](#), GEOVIDE stations 32, 38, 44 (values in brackets indicate hydrothermal influence inferred by those authors).

b. Southern Ocean >200 m, mean of all data from [Sieber et al. \(2020\)](#) and [Wang et al. \(2018\)](#).

c. [Sieber et al. \(2020\)](#), ACE station 20.

d. [Conway and John \(2014\)](#). Carter: USGT10-11 and 10-10. Manning: USGT11-8, 11-10.

e. [Samanta et al. \(2017\)](#), Tasman Sea stations P2 and P3.

f. [Heller and Croot \(2015\)](#), stations 249, 236.

g. [Roshan and Wu \(2015\)](#), USGT10-11, USGT11-10.

h. [Thompson and Ellwood \(2014\)](#), Tasman Sea station P3.

x. Surface ocean estimate for Melville Bank coral based on approximate range of deep water δ⁶⁶Zn values.

IDP17: [Schlitzer et al. \(2018\)](#).

3. Results

3.1. Cleaning experiments

Illustrative results from the cleaning experiments are presented in [Fig. 3](#) (Tasmanian coral SS0108) and [Fig. 4](#) (Drake Passage coral DH115-DC-01), with the complete dataset given in [Table 2](#) and further metal/Ca ratio cross-plots in [Fig. S1](#) and [S2](#). Trace element/calcium ratios decrease with progressive cleaning, with Zn/Ca and Cu/Ca ratios in fully cleaned samples a factor of 5–10 lower than in uncleaned samples, and two to three orders of magnitude lower than in the coral coatings ([Figs. 3, 4](#), [S1](#), [S2](#); [Table 2](#)). Copper is most closely correlated with Mn concentrations, and Zn with Fe concentrations, but strong correlations exist between all four elements, and with Al ([Figs. 3, 4](#), [S1](#), [S2](#)). As a result, distinguishing the contributions of Fe oxides, Mn oxides, and detrital contaminants on the basis of metal/Ca ratios is precluded.

Coating δ⁶⁵Cu values (−0.01‰, +0.23‰) are more negative than cleaned coral aragonite, consistent with Cu derived from a mixed lithogenic (i. e. detrital silicates, at about 0‰; [Moynier et al., 2017](#)) and/or authigenic Fe-Mn oxide source (at about +0.3‰; [Albarède, 2004](#); [Little et al., 2014, 2017](#)). Coating δ⁶⁶Zn values (+0.55‰, +0.25‰) can be either more positive or negative than coral aragonite, reflecting the diverse Zn isotope compositions in potential contaminating material. The Zn isotope composition of lithogenic (i. e. detrital silicates) and authigenic Fe-Mn oxide sources are expected to be about +0.3‰ ([Moynier et al., 2017](#)) and +1‰ ([Maréchal et al., 2000](#); [Little et al., 2014](#)), respectively.

Fully cleaned coral Cu concentrations for the two cleaning specimens are 0.2 to 0.4 μg/g, with Cu/Ca ratios of 0.4 to 0.7 μmol/mol and δ⁶⁵Cu

values ranging from +0.69 to +0.89‰. Fully cleaned Zn concentrations are 0.37 to 0.67 μg/g, with Zn/Ca ratios of 0.38 to 0.68 μmol/mol and δ⁶⁶Zn values of +0.34 to +0.40‰. For these two coral specimens, thorough physical cleaning appears to be effective in removing Zn associated with the coating, leading to similar results to those of fully chemically cleaned samples ([Figs. 3 and 4](#), C and D). Interestingly, [Wilson et al. \(2017\)](#) also found that physical cleaning is more important than chemical cleaning for removing anthropogenic Pb from fossil corals. In contrast, the full cleaning procedure has a marked impact on Cu/Ca and δ⁶⁵Cu of the Tasmanian coral compared to the physically cleaned and oxidatively cleaned aliquots ([Fig. 3A and B](#)).

Finally, the fully cleaned Zn and Cu isotope compositions of both corals subject to cleaning experiments are comparable to modern day seawater Zn (δ⁶⁶Zn = +0.45 ± 0.14‰, 2SD, data >200 m in Southern Ocean or >600 m elsewhere; [Conway and John, 2014, 2015](#); [Zhao et al., 2014](#); [Samanta et al., 2017](#); [John et al., 2018](#); [Vance et al., 2019](#); [Lemaitre et al., 2020](#); [Liao et al., 2020](#); [Sieber et al., 2020](#)) and Cu (δ⁶⁵Cu = +0.66 ± 0.19‰, 2SD, data >200 m; [Takano et al., 2014](#); [Thompson and Ellwood, 2014](#); [Little et al., 2018](#)) isotope compositions ([Figs. 3 and 4](#)). We also note that Zn/Ca ratios in cleaned samples vary by a factor of two for the Drake Passage coral, with no associated variability in δ⁶⁶Zn ([Fig. 4C and D](#)).

3.2. Holocene corals

3.2.1. Trace element/Ca ratios

For the fully cleaned Holocene coral samples, indicators of detrital or Fe-Mn oxide contamination (Fe/Ca, Mn/Ca, Al/Ca) are very low ([Fig. S3](#); [Table 3](#)), with the exception of coral #17 from the northwest Atlantic

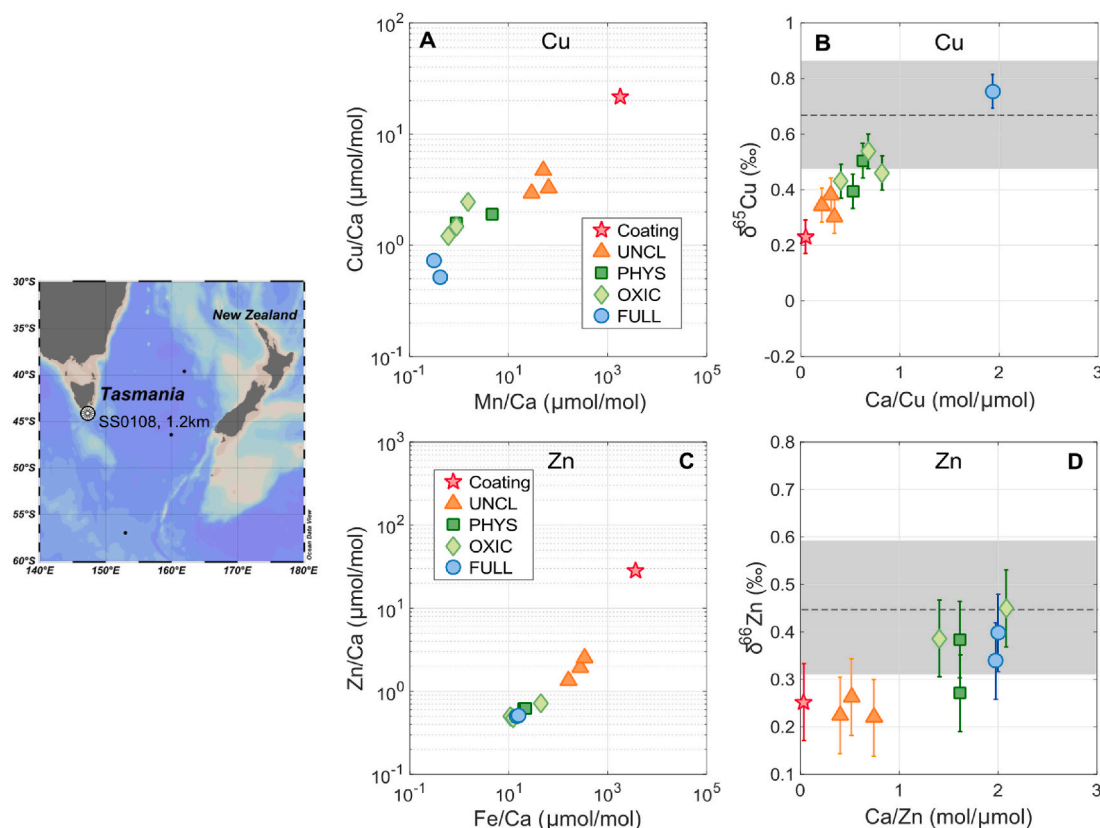


Fig. 3. Illustrative results of the cleaning experiment on Tasmanian coral sample SS0108. Inset map shows location of the coral and its water depth. Panels A and C show Cu/Ca and Zn/Ca ratios of the cleaning aliquots versus trace element indicators of contamination (Mn/Ca and Fe/Ca respectively); note log-log scales. Panels B and D show $\delta^{65}\text{Cu}$ and $\delta^{66}\text{Zn}$ values versus the inverse of their concentration, as Ca/Cu and Ca/Zn respectively. Dashed lines and grey bars represent the average and 2SD range of modern deep seawater ($\delta^{66}\text{Zn} = +0.45 \pm 0.14\text{‰}$; $\delta^{65}\text{Cu} = +0.66 \pm 0.19\text{‰}$; see text for references). Red stars represent the coral coating, orange triangles: uncleaned coral aliquots, dark green squares: physically cleaned aliquots, light green diamonds: physically and oxidatively pre-cleaned aliquots, and blue circles: fully cleaned samples.

(particularly sub-sample B). This sample remained visibly unclean after physical cleaning and has somewhat elevated Fe/Ca (6.7 and 15.2 $\mu\text{mol/mol}$ for sub-samples A and B) and Al/Ca ratios (14.7 $\mu\text{mol/mol}$ and 28.5 $\mu\text{mol/mol}$). Other samples typically exhibit Fe/Ca ratios < 2 $\mu\text{mol/mol}$ (max: 3.8 $\mu\text{mol/mol}$), Mn/Ca ratios < 0.25 $\mu\text{mol/mol}$ (max: 0.48 $\mu\text{mol/mol}$), and Al/Ca ratios that are below detection (max: 3.1 $\mu\text{mol/mol}$). By contrast, coral coatings exhibit Mn/Ca, Fe/Ca, and Al/Ca ratios that are very variable (due to the variable carbonate content of the scrapings), but in all cases several orders of magnitude higher than those of the cleaned corals (Table 3). For comparison, Marchitto and Broecker (2006) compiled values for chemically cleaned benthic foraminifera of 4–51 (Fe/Ca) and 11–68 (Mn/Ca) $\mu\text{mol/mol}$, and Marchitto et al. (2005) limited palaeoceanographic interpretation of benthic foraminiferal Zn/Ca data to samples with Mn/Ca values of < 200 $\mu\text{mol/mol}$. Hence, the Fe/Ca and Mn/Ca ratios of our corals are typically at least an order of magnitude lower (up to three orders of magnitude lower for Mn/Ca) than those in foraminifera-based studies.

Cleaned samples of *D. dianthus* exhibit Zn/Ca ratios in a fairly tight range of 0.4 to 3.0 $\mu\text{mol/mol}$, while samples of *Caryophyllia* and *Dasmosmilia* spp. have much more variable and sporadically high Zn/Ca (range 0.3–17 $\mu\text{mol/mol}$; Table 3, Figs. 5, S3). No discernible species-related variability in Cu/Ca ratios is observed, with all samples in the range of 0.13 to 1.0 $\mu\text{mol/mol}$ (Table 3, Figs. 5, S3). No relationships between Zn/Ca or Cu/Ca and Fe/Ca, Mn/Ca, or Al/Ca are present in the Holocene coral dataset (Fig. S3; Table 3). For the two sub-samples of coral #17, which exhibit elevated Fe/Ca and Al/Ca, Zn/Ca and Cu/Ca ratios are some of the lowest of the whole dataset (Zn/Ca: 0.52, 0.58 $\mu\text{mol/mol}$; Cu/Ca: 0.16, 0.22 $\mu\text{mol/mol}$).

3.2.2. Holocene coral $\delta^{66}\text{Zn}$ and $\delta^{65}\text{Cu}$ values

All fully cleaned coral duplicates are within analytical uncertainty for $\delta^{66}\text{Zn}$ and $\delta^{65}\text{Cu}$, based on the external 2SD reproducibility obtained for multiple analyses of a carbonate standard ($\pm 0.07\text{‰}$ and $\pm 0.11\text{‰}$ respectively; Table 4). However, the results from duplicate analyses of sample #1 (Reykjanes Ridge) are at the limit of this definition of the uncertainty, both for $\delta^{66}\text{Zn}$ ($+0.67\text{‰}$, $+0.55\text{‰}$) and $\delta^{65}\text{Cu}$ ($+0.45\text{‰}$, $+0.25\text{‰}$). The two sub-samples of coral #17, with variably elevated Fe/Ca and Al/Ca (Table 3), are analytically indistinguishable in both $\delta^{66}\text{Zn}$ ($+0.61\text{‰}$, $+0.54\text{‰}$) and $\delta^{65}\text{Cu}$ ($+0.62\text{‰}$, $+0.54\text{‰}$).

Coral coatings exhibit $\delta^{66}\text{Zn}$ values of $+0.25$ to $+0.90\text{‰}$ and $\delta^{65}\text{Cu}$ values of -0.01 to $+0.26\text{‰}$ (Table 4), consistent with mixtures of detrital and authigenic Zn and Cu (as seen in the cleaning experiments). Coatings are also distinctly different in isotopic composition compared to their respective corals: both higher and lower $\delta^{66}\text{Zn}$ values are observed in coatings compared to corals, while $\delta^{65}\text{Cu}$ values are always lower in coatings (Table 4).

Fig. 5 presents cleaned coral Zn and Cu isotope compositions compared to Ca/Zn and Ca/Cu ratios respectively, with data differentiated by species or genera. The spread in Holocene coral $\delta^{66}\text{Zn}$ values is from $+0.07$ to $+0.67\text{‰}$, with $\delta^{65}\text{Cu}$ values of $+0.27$ to $+1.05\text{‰}$. No systematic species-specific isotopic variability is evident in these small datasets (Fig. 5). Most samples overlap the range of modern deep ocean isotopic compositions (shaded blue bars) for Zn ($+0.45 \pm 0.14\text{‰}$, 2SD, data > 200 m in Southern Ocean or > 600 m elsewhere; Conway and John, 2014, 2015; Zhao et al., 2014; Samanta et al., 2017; John et al., 2018; Vance et al., 2019; Lemaître et al., 2020; Liao et al., 2020; Sieber et al., 2020) and Cu ($+0.66 \pm 0.19\text{‰}$, 2SD, data > 200 m; Takano et al.,

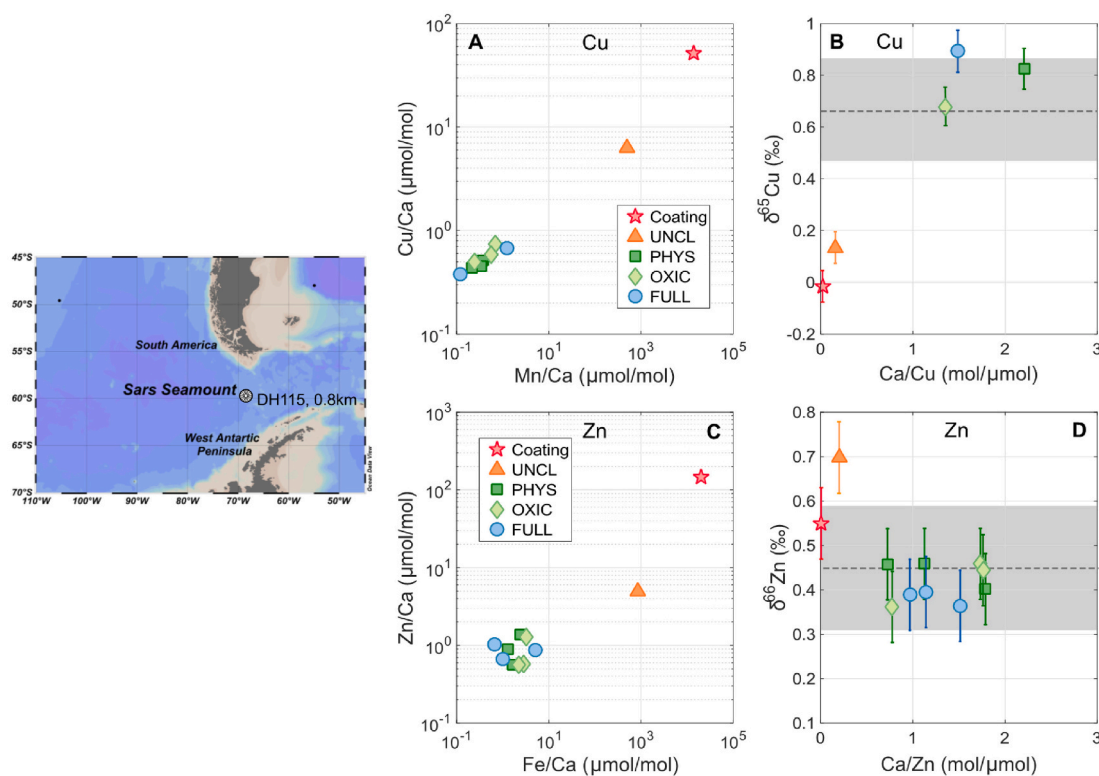


Fig. 4. Illustrative results of the cleaning experiment on Drake Passage coral sample DH115-DC-01. Inset map shows location of the coral, from Sars Seamount, and its water depth. Panels A and C show Cu/Ca and Zn/Ca ratios of the cleaning aliquots versus trace element indicators of contamination (Mn/Ca and Fe/Ca respectively); note log-log scales. Panels B and D show $\delta^{65}\text{Cu}$ and $\delta^{66}\text{Zn}$ values versus the inverse of their concentration, as Ca/Cu and Ca/Zn respectively. Dashed lines and grey bars represent the average and 2SD range of modern deep seawater ($\delta^{66}\text{Zn} = +0.45 \pm 0.14\%$; $\delta^{65}\text{Cu} = +0.66 \pm 0.19\%$; see text for references). Symbols are as in Fig. 3.

2014; Thompson and Ellwood, 2014; Little et al., 2018). There is some indication of a weak trend in Ca/Zn versus $\delta^{66}\text{Zn}$, with isotopically heavier Zn broadly linked to samples with lower Zn concentrations (i. e. higher Ca/Zn ratios).

3.3. Glacial corals

Indicators of detrital or authigenic Fe-Mn oxide contamination for the four *D. dianthus* specimens from the last glacial period are slightly elevated compared to the Holocene dataset, but remain low overall (Table 3). Glacial coral Al/Ca ratios range from below detection to 16.1 $\mu\text{mol/mol}$, Fe/Ca ratios from 2.0 to 13.3 $\mu\text{mol/mol}$, and Mn/Ca ratios from 0.1 to 1.2 $\mu\text{mol/mol}$. The ranges of glacial coral Zn/Ca (0.6 to 3.0 $\mu\text{mol/mol}$) and Cu/Ca (0.2 to 0.5 $\mu\text{mol/mol}$) ratios are very similar to their Holocene counterparts (Table 3; Fig. 5).

Isotopically, corals from the last glacial period overlap with the respective Holocene datasets, with the exception of a single sample from the equatorial Atlantic (sample #20) that expands the measured $\delta^{66}\text{Zn}$ range to $+0.79\%$ (Fig. 5; Table 4). The two North Atlantic corals have more positive $\delta^{66}\text{Zn}$ values ($+0.79\%$, $+0.67\%$) than the corals from the Southern Ocean and Tasman Sea ($+0.37\%$, $+0.38\%$). The range in $\delta^{65}\text{Cu}$ values for the four glacial specimens is from $+0.66\%$ to 0.84% , with no systematic geographical variability (Table 4).

4. Discussion

4.1. Zn and Cu partitioning in cold-water coral aragonite

Best estimates for ambient seawater Zn and Cu concentrations were compiled by extrapolating along isopycnals from the nearest seawater profile or, in the southwest Indian Ocean where data is sparse, the most

oceanographically equivalent profile based on proximity to Southern Ocean fronts (Fig. 1, Table 4). Assuming that Ca is uniformly distributed in the ocean at a concentration of $10.3 \text{ mmol kg}^{-1}$, we calculate apparent partition coefficients for each coral specimen as follows (Table 4):

$$D_{\text{Zn}} = [\text{Zn/Ca}]_{\text{coral}} / [\text{Zn/Ca}]_{\text{seawater}} \quad (3)$$

$$D_{\text{Cu}} = [\text{Cu/Ca}]_{\text{coral}} / [\text{Cu/Ca}]_{\text{seawater}} \quad (4)$$

Note that reported Zn concentrations in and around the active hydrothermal vent site of the Reykjanes Ridge range widely from 1.4 to 6 nmol/kg (Lemaitre et al., 2020), while Cu concentrations at this location are poorly defined. Previous work has also found that Ba partitioning in these Icelandic corals is unusual compared to corals from elsewhere in the Atlantic and Southern Ocean, indicating a possible site-specific effect in this location (Hemsing et al., 2018; Spooner et al., 2018). Therefore, the two Icelandic corals are excluded from the description of elemental partitioning that follows.

Zinc and Cu partitioning in *D. dianthus* specimens is generally uniform, with $D_{\text{Zn}} = 4.4 \pm 2.2$ (2SD; excluding Icelandic corals), and $D_{\text{Cu}} = 1.4 \pm 1.0$ (2SD; excluding Icelandic corals and sample #21 with $D_{\text{Cu}} = 6.4$). Calculated D_{Zn} values for *Caryophyllia* and *Dasmosmilia* are generally elevated and more variable than those of *D. dianthus*, ranging between 3.1 and 92 (Table 4). Similarly, calculated D_{Cu} values for *Caryophyllia* and *Dasmosmilia* are also more variable than for *D. dianthus*, at 0.9 to 10.

We also observe significant intra-coral variability in Zn/Ca and Cu/Ca ratios for specimens that were separately sub-sampled and analysed more than once. For example, for the glacial-age Drake Passage coral DH115-DC-01, which was subject to the cleaning experiment and thus analysed on multiple occasions, the range in Zn/Ca ratios for all

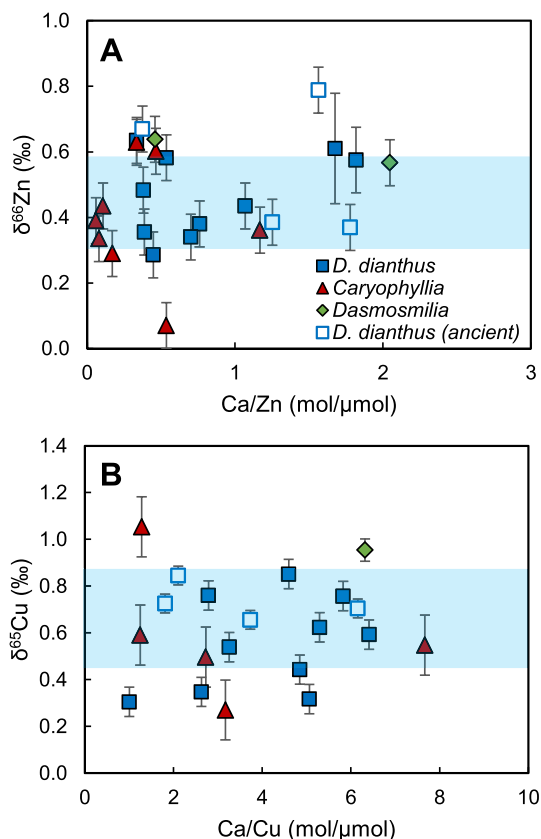


Fig. 5. Coral (A) Zn and (B) Cu isotope compositions versus Ca/Zn and Ca/Cu ratios respectively (mol/ μ mol), illustrated by species. Filled blue squares: Holocene *D. dianthus*; filled red triangles: *Caryophyllia*; filled green diamonds: *Dasmosmia*; unfilled blue squares: *D. dianthus* from the last glacial period. Blue bars represent the 2SD range of modern deep seawater ($\delta^{66}\text{Zn} = +0.45 \pm 0.14\%$; $\delta^{65}\text{Cu} = +0.66 \pm 0.19\%$; see text for references). Average Zn/Ca and Cu/Ca ratios and isotopic compositions are plotted for samples measured in duplicate. Error bars on isotope ratios are the external 2SD reproducibility of a secondary carbonate standard ($\delta^{66}\text{Zn} \pm 0.07\%$, $\delta^{65}\text{Cu} \pm 0.11\%$), the 2SD on duplicate sample measurements, or the internal 2SE of the isotopic analysis, whichever is larger.

‘cleaned’ samples (i. e. all physically and chemically cleaned samples, $n = 12$) is 0.37–0.90 $\mu\text{mol/mol}$. For the ‘fully cleaned’ samples only ($n = 4$), the Zn/Ca range is similar, at 0.38–0.68 $\mu\text{mol/mol}$. For Cu, the equivalent intra-specimen variability is 0.37–0.80 $\mu\text{mol/mol}$ for all ‘cleaned’ samples, or 0.37–0.67 $\mu\text{mol/mol}$ for ‘fully cleaned’ samples. Taken at face value, such differences would imply intra-coralline variability in D_{Zn} and D_{Cu} for *D. dianthus* of approximately a factor of two, similar to the variability in partitioning between individual specimens (Fig. 6).

Intra-coralline variability could be structural, since differences in trace element/Ca ratios have been observed between centres of calcification (COC) and regions of fibrous aragonite. For example, Mg/Ca and Li/Ca ratios are significantly enriched in COCs (Gagnon et al., 2007; Meibom et al., 2008; Case et al., 2010; Anagnostou et al., 2011). This variability has been proposed to reflect either Rayleigh fractionation processes (e.g., Gagnon et al., 2007; Case et al., 2010) or differences in precipitation rate, with COCs precipitating more rapidly than fibrous regions (Gabitov et al., 2008; Brahmi et al., 2012). It has also been suggested that Mg may be more easily incorporated into organic compounds or amorphous calcium carbonate than substituted for Ca in the aragonite lattice, with the former components both thought to be more prevalent in COCs than surrounding fibres (Cuif et al., 2003; Finch and Allison, 2008; Rollion-Bard et al., 2010). Since sub-samples of individual

coral specimens can be expected to include carbonate from COCs and fibrous regions in differing proportions, the observed intra-specimen variability in Zn and Cu concentrations hints at similar controls on the partitioning of these elements. Hence, future work should employ high sensitivity, microanalytical techniques to evaluate the distribution of Zn and Cu in COCs versus fibrous aragonitic regions of cold-water corals.

4.2. Comparison of cold-water coral and seawater Zn and Cu isotope compositions

Most Holocene cold-water coral $\delta^{66}\text{Zn}$ values are within uncertainty of ambient seawater $\delta^{66}\text{Zn}$ values (Figs. 5, 7). For each specimen, the parameter $\Delta^{66}\text{Zn}_{\text{coral-sw}}$ is calculated, where:

$$\Delta^{66}\text{Zn}_{\text{coral-sw}} = \delta^{66}\text{Zn}_{\text{coral}} - \delta^{66}\text{Zn}_{\text{seawater}} \quad (5)$$

For the complete Holocene dataset, we find $\Delta^{66}\text{Zn}_{\text{coral-sw}} = +0.03 \pm 0.17\%$ (1SD, $n = 20$) (Fig. 8; Table 4). Therefore, the first order finding of this study is that coral aragonite appears to incorporate Zn from seawater without isotopic fractionation. In addition, live-collected and fossil Holocene corals from similar depths overlap in $\Delta^{66}\text{Zn}_{\text{coral-sw}}$, with no perceptible diagenetic modification of coral Zn isotope compositions (Fig. 8). Furthermore, at the resolution of this study (i. e. bulk analysis of ca. 100 mg coral aliquots), intra-coralline variability in Zn/Ca (section 4.1) is not associated with resolvable variability in $\delta^{66}\text{Zn}$ (Figs. 3, 4).

However, the dataset exhibits some scatter in $\Delta^{66}\text{Zn}_{\text{coral-sw}}$, with several specimens that exhibit higher or lower $\delta^{66}\text{Zn}$ values compared to ambient seawater (Figs. 7, 8). The simplest explanation for scatter in $\Delta^{66}\text{Zn}_{\text{coral-sw}}$ would be the presence of Zn from residual contaminating phases, i. e. Fe-Mn oxides or detrital grains. For those corals with a well-developed coating, the contribution from any residual coating to the Zn budget of a cleaned coral can be estimated as follows:

$$[\text{Zn}]_{\text{coating contribution}} = [\text{Fe}]_{\text{coral}} \times \left(\frac{\text{Zn}}{\text{Fe}} \right)_{\text{coating}} \quad (6)$$

In this equation, Zn can be replaced by Cu, and Fe can be replaced by another indicator of contamination, such as Mn. Coating Zn contributions of 0.0–3.0% based on Fe (or 0.0–3.6% based on Mn) are calculated for seven of eight corals (Table S3). For a single glacial-age sample (SS0108), this approach yields an estimate of 21% based on Fe (or 1.2% based on Mn) (Table S3). For Cu, the equivalent coating contributions are 0.4–14% based on Fe (or 0.0–17% based on Mn). Mass balance can then be applied to correct the measured isotopic compositions of cleaned corals using paired coral and coating $\delta^{66}\text{Zn}$ and $\delta^{65}\text{Cu}$ values (Table S3). In all cases, the corrected and uncorrected isotopic compositions overlap within measurement uncertainty, with a maximum correction of $+0.03\%$ for Zn and $+0.08\%$ for Cu (in both cases for the glacial coral SS0108, based on Fe). It therefore appears unlikely that the observed scatter in $\Delta^{66}\text{Zn}_{\text{coral-sw}}$ (Fig. 8) can be the result of residual contaminating phases.

One observation that may indicate a systematic rather than random occurrence of samples with a $\Delta^{66}\text{Zn}_{\text{coral-sw}}$ offset is that the three corals from the upper 0.5 km of the water column (samples #10 and #11 from the eastern equatorial Atlantic, #13 from the SW Indian Ocean; Table 4) have positive $\Delta^{66}\text{Zn}_{\text{coral-sw}}$ values (i. e. they are isotopically heavier than seawater; Fig. 8). A possible explanation for these offsets is that the estimates of ambient seawater $\delta^{66}\text{Zn}$ values are inaccurate; to explain positive coral $\Delta^{66}\text{Zn}_{\text{coral-sw}}$ values, the seawater values must be too low. This scenario is most likely to arise for the upper water column, where seawater $\delta^{66}\text{Zn}$ values are highly variable and, outside of the Southern Ocean, excursions towards low sub-surface $\delta^{66}\text{Zn}$ values are frequently observed (e.g., see Fig. 7; Conway and John, 2014; Samanta et al., 2017; Vance et al., 2019; Lemaître et al., 2020; Liao et al., 2020). The origin of these isotopically light excursions is a subject of active debate, but a link to anthropogenic aerosol input has been proposed (Lemaître et al., 2020; Liao et al., 2020), which would imply that they are a recent

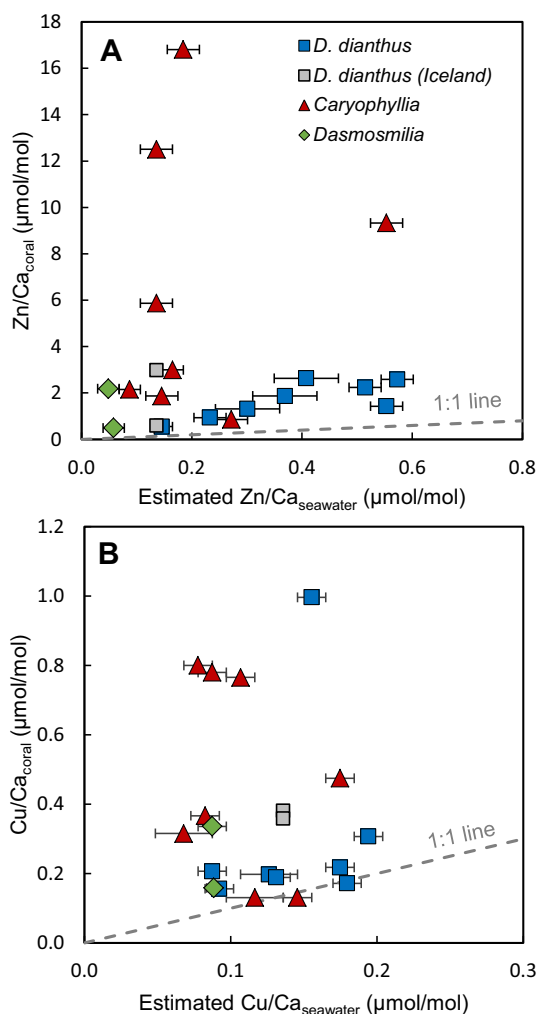


Fig. 6. (A) Comparison of Holocene coral Zn/Ca ratios with estimated ambient seawater Zn/Ca ratios (for references, see Table 4) and (B) coral Cu/Ca ratios with estimated seawater Cu/Ca ratios, by coral species. Mean Zn/Ca_{coral} and Cu/Ca_{coral} ratios are plotted for samples analysed in duplicate or triplicate. Blue squares: *D. dianthus*; red triangles: *Caryophyllia*; green diamonds: *Dasmosmilia*. Grey squares are *D. dianthus* specimens from Iceland, for which ambient seawater Zn and Cu concentrations (and thus Zn/Ca and Cu/Ca) are poorly constrained; for example, reported Zn concentrations at stations close to the Reykjanes Ridge range from 1.4 to 6 nmol/kg (Lemaitre et al., 2020). Grey dashed lines represent partition coefficients of 1 (e.g., Zn/Ca_{coral} = Zn/Ca_{seawater}).

phenomenon. Estimated cold-water coral growth rates are on the order of 0.5–2 mm/yr (Adkins et al., 2004), hence a single isotope analysis is likely to represent a few decades to a century of coral growth. Therefore, even though two of the three upper water column corals in this study were collected alive, it is plausible that all three corals lived a substantial portion of their lives in seawater with a Zn isotope composition that was heavier than observed in the modern-day.

Two fossil samples from deeper water have negative $\Delta^{66}\text{Zn}_{\text{coral-sw}}$ values (#14 at 0.8 km depth from Atlantis Bank in the SW Indian Ocean, #19 at 1.9 km depth from South Hills, Tasmania; Fig. 8, Table 4). Deep seawater $\delta^{66}\text{Zn}$ values are generally homogeneous, so these results are difficult to explain. The isotopic composition of sample #19 from Tasmania is +0.29‰, comparable to the lithogenic Zn isotope composition (at about +0.3‰), but the trace element data provides no indication of detrital contamination (e.g., Al/Ca ratio is below detection; Table 3). Sample #14, from Atlantis Bank, is even lighter, at +0.07‰, and seems to be anomalous as three other corals (#16, #22, #23) from similar

depths (743–1035 m) at Atlantis Bank have values of +0.44‰, +0.29‰ and +0.39‰. These anomalies could potentially derive from the chemical cleaning procedure: several studies have suggested that the inclusion of a reductive cleaning step can lead to analytical artefacts (Pichat et al., 2003; Yu et al., 2007; Clarkson et al., 2020), including anomalous shifts to more negative $\delta^{66}\text{Zn}$ values in carbonates (Druce, 2021).

To fully resolve the origin of the observed positive (and occasional negative) $\Delta^{66}\text{Zn}_{\text{coral-sw}}$ values, and the extent to which they represent a potential source of new information versus a limitation of the proxy archive, will require a larger dataset of cold-water coral data and better observational constraints on water column Zn isotope variability. In addition, the future collection of contemporaneous coral and seawater samples would enable a more direct comparison between fluid and solid compositions, thereby reducing uncertainties and improving the ability to test models of trace metal uptake and isotopic fractionation in corals.

The availability of local seawater Cu isotope data is much more limited than for Zn, which restricts us to a global-scale comparison between coralline and seawater $\delta^{65}\text{Cu}$ values. The average of the Holocene cold-water coral $\delta^{65}\text{Cu}$ dataset is $+0.59 \pm 0.23\text{‰}$ (1SD, $n = 15$), comparable to the mean of published deep seawater $\delta^{65}\text{Cu}$ values, at $+0.66 \pm 0.09\text{‰}$ (1SD, $n = 119$, all data >200 m; Takano et al., 2014; Thompson and Ellwood, 2014; Little et al., 2018). However, there is considerably more variability in the coral $\delta^{65}\text{Cu}$ values, which range from +0.27 to +1.05‰, than is typically observed in the deep ocean (Figs. 5, S4). Unless this variability reflects undiagnosed analytical artefacts (section 2.3), the presence of residual contaminating phases (which is not supported by mass balance calculations), or an influence from the chemical cleaning procedure (e.g., Yu et al., 2007; Druce, 2021), it suggests complexity in the mechanisms of Cu incorporation in coral aragonite.

Notably, the biogeochemistry of Cu and Cu isotopes, including Cu sorption and incorporation in calcite, is strongly influenced by organic complexation (McBride, 1981; Coale and Bruland, 1988; Lee et al., 2005; Ryan et al., 2014), and up to 2.5% by weight of live coral skeletons comprises organic material (plus associated water) (Cuif et al., 2004). It is interesting that the four coral specimens from the last glacial period are rather more homogeneous in their Cu isotope compositions (+0.66‰, +0.70‰, +0.73‰, +0.84‰) than the Holocene dataset, which could perhaps relate to the degradation of organics over time. However, we observe no relationship between coral age and $\delta^{65}\text{Cu}$ values for the Holocene and live-collected corals (Fig. S5), and so this hypothesis remains speculative. Further experimental, observational, and seawater Cu isotope analyses are required to better interpret the small dataset of cold-water coral Cu isotope compositions that is presented here as a starting point for any future endeavour.

4.3. Inorganic versus biogenic carbonate precipitation

For elemental ratios and isotopic compositions in carbonates to be useful paleoenvironmental tools, they should be free of so-called ‘vital effects’, or the impact of such vital effects should be systematic and quantifiable. This section considers in greater depth the possible inorganic controls and the influence of vital effects on coral Zn/Ca, Cu/Ca, $\delta^{66}\text{Zn}$, and $\delta^{65}\text{Cu}$ values. We focus primarily on Zn because more information exists with which to evaluate the partitioning and isotope fractionation of Zn than Cu in carbonates.

4.3.1. Partitioning behaviour

Biogenic partition coefficients are not directly comparable to the thermodynamic framework developed for inorganic precipitation, because carbonate biomineralization is strongly organism-controlled (e.g., Elderfield et al., 1996). Foraminifera are thought to calcify via transmembrane transport and/or seawater vacuolization (De Nooijer et al., 2014), while scleractinian corals calcify from a so-called ‘extracellular calcifying fluid’ (ECF) (Adkins et al., 2003; Cohen and McConaughy, 2003; Allemand et al., 2004). Nevertheless, comparisons to

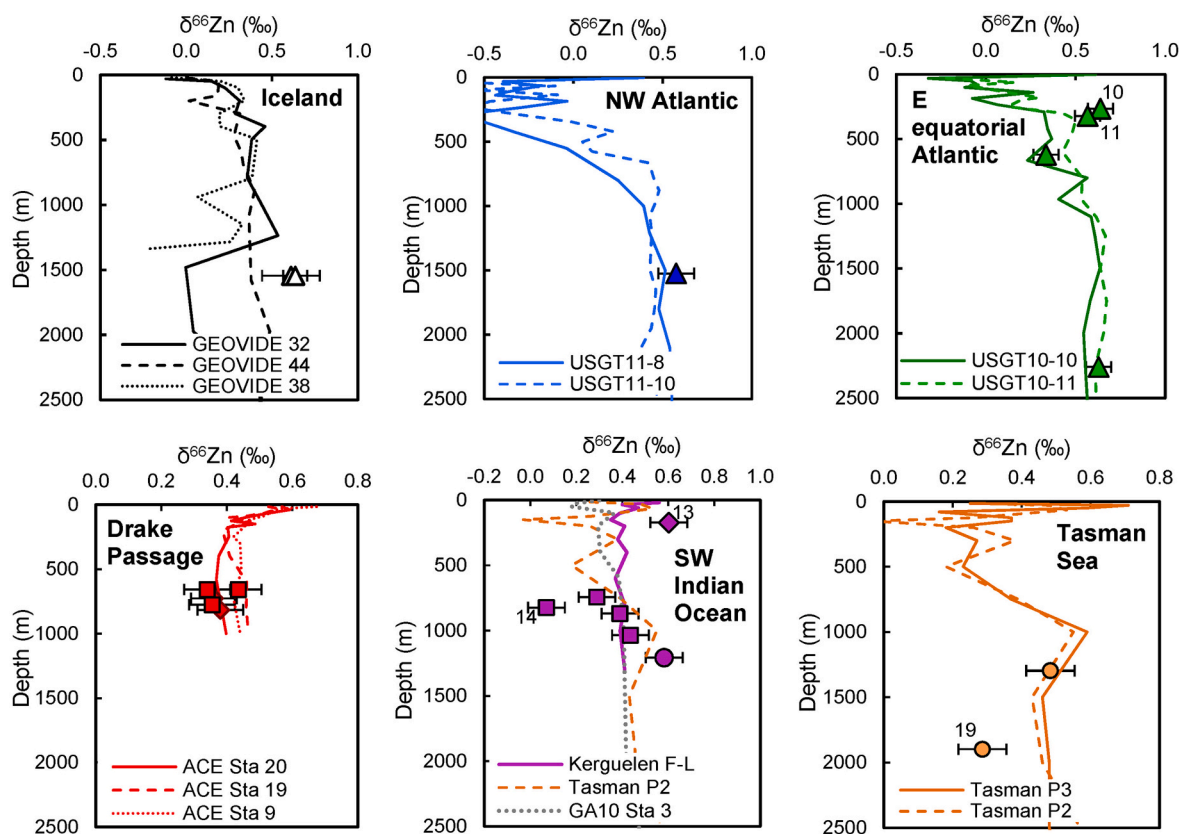


Fig. 7. Zinc isotope composition of Holocene corals versus water depth, plotted by geographic location. Atlantic corals are shown by triangles. Open triangles: Reykjanes Ridge, Iceland; blue triangle: Manning Seamount, NW Atlantic; green triangles: Carter Seamount, eastern equatorial Atlantic. Drake Passage corals are red squares (Sars Seamount) and red diamonds (Burdwood Bank). SW Indian Ocean corals are purple squares (Atlantis Bank), diamond (Melville Bank) or circle (Coral Seamount). Tasmanian corals are orange circles. Local or most oceanographically equivalent seawater profiles (determined by water mass comparisons and neutral density estimates) are shown in solid, dashed, or dotted lines (individual panel legends, see Fig. 1 and Table 4 for locations and references). Corals discussed in the text (i. e. those notably offset from ambient seawater) are labelled with their respective sample numbers (see also Fig. 8).

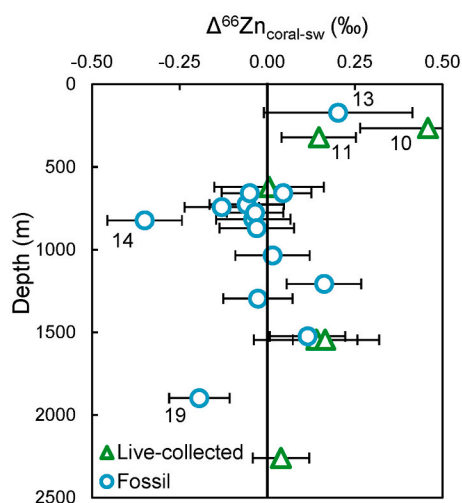


Fig. 8. The offset between Holocene coral and ambient seawater $\delta^{66}\text{Zn}$ values, reported as $\Delta^{66}\text{Zn}_{\text{coral-sw}}$, versus water depth. Live-collected corals are shown as green triangles, with fossil corals shown as blue circles. Error bars are the propagated uncertainty from coral and seawater compositions. Corals discussed in the text (i. e. those notably offset from seawater values) are labelled with their respective sample numbers (see also Fig. 7).

inorganic systems can still be instructive.

Inorganic trace element partitioning experiments for calcium carbonates have focused on calcite, in which Zn^{2+} and Cu^{2+} ions first adsorb on the mineral surface before substituting isomorphously for octahedrally coordinated Ca^{2+} in the mineral structure (Reeder et al., 1999; Elzinga and Reeder, 2002). The resulting inorganic partition coefficients for Zn in calcite (see section 4.1) are generally high, ranging from ~ 5 to >100 (Crocket and Winchester, 1966; Kitano et al., 1980; Rimstidt et al., 1998; Temmam et al., 2000; Mavromatis et al., 2019). Using ab initio methods, Menadakis et al. (2007, 2009) calculated that Zn^{2+} substitution for Ca^{2+} is more energetically favourable in calcite than in aragonite, consistent with experimental results from Kitano et al. (1973, 1980), which showed that Zn partition coefficients are a factor of 10 lower for aragonite than for calcite (5 for aragonite cf. 50 for calcite). Fewer studies have investigated Cu partitioning in carbonates, but estimated partition coefficients are in a similar range to Zn (~ 20 – 80 for calcite; Kitano et al., 1980; Rimstidt et al., 1998) and are also a factor of 10 lower for aragonite than calcite (e.g., 2.5 for aragonite cf. 25 for calcite; Kitano et al., 1973). Such variability in inorganic partitioning likely reflects the wide range of physical and chemical parameters, such as temperature, pressure, salinity, metal concentration, pH, and calcite saturation state, that can all influence partitioning behaviour (recently reviewed by Smrzka et al., 2019).

In culture, calcitic benthic foraminifera exhibit partition coefficients for both Zn and Cu that are lower compared to inorganic values for calcite. Van Dijk et al. (2017) calculated foraminiferal calcite D_{Zn} values of 0.7 to 1.9 (*Ammonia tepida*), and similar values of 0.2 to 4.0 were estimated for *Pseudotriloculina rotunda* (Nardelli et al., 2016). Munsel

et al. (2010) determined a D_{Cu} value of 0.14 ± 0.02 for *A. tepida*, similar to the estimate of 0.25 ± 0.15 for *A. tepida* and *Heteristegina depressa* (de Nooijer et al., 2007). These low partition coefficients may in part be explained by the presence in the culture media of other dissolved species such as Cl^- or organic complexes at higher concentrations than in the inorganic experiments described above; both were shown to reduce inorganic partitioning (Temmam et al., 2000; Lee et al., 2005). In addition, the mechanism of incorporation may influence partitioning: active uptake of metals over a membrane may be less favourable than sorption directly on the mineral surface in inorganic experiments (De Nooijer et al., 2014; van Dijk et al., 2017).

In the field, benthic foraminifera from ocean sediment core tops have estimated D_{Zn} values of ~ 9 (*Cibicoides wuellerstorfi*; Marchitto et al., 2000) and ~ 22 (*Cibicoides pachyderma*; Bryan and Marchitto, 2010), which are higher compared to cultured specimens but similar to the range observed in inorganic calcite experiments. Zinc partitioning in cultured foraminifera is also sensitive to Zn concentrations, with the highest partition coefficients arising at low Zn concentrations that are more comparable to natural seawater (Nardelli et al., 2016). Such an effect may explain the higher Zn partitioning in field-collected benthic foraminifera. Alternatively, or in addition, differences between field-collected and cultured foraminifera may result from species-specific vital effects, contamination of field-collected samples, or additional environmental controls on Zn incorporation (e.g., growth rate) (van Dijk et al., 2017).

Coral calcification occurs via the up-regulation of pH and aragonite saturation state in the ECF. This up-regulation is achieved via an enzymatic alkalinity pump (a Ca^{2+} -ATPase), which removes 2 protons for every Ca^{2+} ion pumped in (Ip et al., 1991; Al-Horani et al., 2003). As a result, dissolved inorganic carbon speciation shifts towards CO_3^{2-} and aragonite saturation state increases, which in turn aids aragonite precipitation. The observed partition coefficients for cold-water corals cover a wide range (Table 4), particularly those for Zn in *Caryophyllia* (3.1 to 92), which span almost the entire range of measured inorganic and benthic foraminiferal values. We find no trace element evidence for residual contaminating phases (section 4.2) that could explain sporadic high D_{Zn} and D_{Cu} values. Instead, we suggest that the spread towards high values is a function of the high inorganic partition coefficients for Zn and Cu in aragonite coupled to variations in coral calcification efficiency.

Following Gagnon et al. (2012), calcification efficiency is defined as the balance between the supply of ions to the ECF from seawater and their removal via $CaCO_3$ precipitation. It can be viewed in terms of either a Rayleigh-type batch reactor (e.g., Gagnon et al., 2007) or a steady-state process (e.g., Gagnon et al., 2012), but the implications for elemental incorporation are similar. Aragonite that is precipitated near the start of a Rayleigh-type removal process, or in a well-flushed ECF reservoir (i. e. low calcification efficiency), will have a high Zn/Ca or Cu/Ca value, reflecting the high inorganic partition coefficients of Zn and Cu. As calcification efficiency increases, either at steady state or following progressive Rayleigh distillation, Zn/ Ca_{coral} and Cu/ Ca_{coral} will approach seawater ratios, and therefore D values of one (grey dashed lines, Fig. 6). We speculate that the calcification efficiency of any individual specimen may reflect site- or species-specific differences. Furthermore, the variable partitioning behaviour observed for *Caryophyllia* may reflect the wide range of species diversity (at least 66 known species; Kitahara et al., 2010a).

4.3.2. Isotopic effects

There have been several experimental studies of Zn isotope fractionation during inorganic incorporation of Zn into or sorption onto carbonate minerals, though not specifically for aragonite. Dong and Wasylenki (2016) showed that the adsorption of Zn onto calcite is associated with a preference for heavy Zn isotopes, with $\Delta^{66}Zn_{CaCO_3-solution}$ values (where $\Delta^{66}Zn_{CaCO_3-solution} = \delta^{66}Zn_{CaCO_3} - \delta^{66}Zn_{solution}$) of $+0.4\text{‰}$ to $+0.7\text{‰}$. They attribute this enrichment in heavy isotopes to a

reduction in coordination number and Zn—O bond length on sorption of octahedrally coordinated Zn^{2+} aquo-complexes as tetrahedral surface complexes (Dong and Wasylenki, 2016). Smaller $\Delta^{66}Zn_{CaCO_3-solution}$ values have generally been observed in co-precipitation experiments. Marechal and Sheppard (2002) estimated a Zn isotope fractionation between smithsonite and fluid of $<0.1\text{‰}$, while Veeramani et al. (2015) found a small preference for light Zn isotopes on precipitation of hydrozincite (-0.18‰). However, Mavromatis et al. (2019) found that Zn isotope fractionation on co-precipitation with calcite is pH dependent, with $\Delta^{66}Zn_{CaCO_3-solution}$ values in their experiments ranging from about 0‰ at pH 8.3 to $+0.6\text{‰}$ at pH 6.1. While not designed to replicate seawater chemistry exactly, their experimental results provide an important demonstration that aqueous Zn speciation and the isotopic fractionation between aqueous species need to be considered in order to explain carbonate $\delta^{66}Zn$ values.

In detail, Mavromatis et al. (2019) attributed the observed decrease in Zn isotope fractionation with increasing pH to an increase in the prevalence of aqueous $ZnHCO_3^+$ and $ZnCO_3^0$ relative to Zn^{2+} . Theoretical *ab initio* calculations predict that $ZnHCO_3^+$ and $ZnCO_3^0$ species are isotopically heavy compared to Zn^{2+} ; therefore, the pool of Zn^{2+} is projected to get both smaller and isotopically lighter with increasing pH (Fujii et al., 2014). Given that the Zn^{2+} species is incorporated into the calcite mineral structure (as a direct substitution for Ca^{2+} ; Elzinga and Reeder, 2002; Elzinga et al., 2006), these changes in speciation should be reflected in the co-precipitation of calcite with a lighter Zn isotope composition and lower D_{Zn} value (Mavromatis et al., 2019). Such an effect does appear to be observed for D_{Zn} values in benthic foraminifera (van Dijk et al., 2017). Based on theoretical calculations, Mavromatis et al. (2019) also show that their experimental data are consistent with a constant offset between Zn in calcite and aqueous Zn^{2+} ($\Delta^{66}Zn_{calcite-Zn^{2+}} = +0.6\text{‰}$) over the full pH range of their experiments. Following Dong and Wasylenki (2016), they attribute this enrichment of heavy Zn isotopes in the mineral phase (relative to aqueous Zn^{2+}) to isotope fractionation during Zn^{2+} sorption to the mineral surface (as per Elzinga and Reeder, 2002; Elzinga et al., 2006; Dong and Wasylenki, 2016), with its subsequent incorporation into the mineral structure proposed to occur without further isotope fractionation (Mavromatis et al., 2019).

In applying the above rationale to the organism-controlled calcification of cold-water corals, it is important to consider the up-regulation of pH in the ECF. Both direct observations (e.g., microsensor and pH-sensitive fluorescent dye) and indirect measurements (e.g., B isotopes) indicate up-regulation on the order of one pH unit above ambient seawater, to about pH 9 to 9.5 (e.g., Al-Horani et al., 2003; Rollion-Bard et al., 2011; Sevilgen et al., 2019). Using geochemical modelling, and also incorporating the effect of complexation of light Zn with the chloride ions found in seawater, Mavromatis et al. (2019) predict $\Delta^{66}Zn_{calcite-sw}$ values of about $+0.3$ to $+0.4\text{‰}$ for precipitation from 'inorganic seawater' at pH 9 to 9.5. Such a prediction clearly contrasts with the cold-water coral dataset presented here, for which $\Delta^{66}Zn_{coral-sw} \approx 0\text{‰}$.

However, Zn speciation in natural seawater (and, presumably, within coral ECF) is more complex than in those inorganic experiments, with a strong influence from complexation to dissolved organic ligands (e.g., Bruland, 1989; Ellwood and Van Den Berg, 2000; Jakuba et al., 2012). Dissolved organic ligands preferentially complex isotopically heavy Zn (Jouvin et al., 2009; Marković et al., 2017). Hence, it is plausible that the small residual Zn^{2+} pool in the ECF is isotopically lighter than would arise in inorganic-only scenarios, which would provide one means to reconcile the predictions of Mavromatis et al. (2019) with the cold-water coral dataset. If this scenario is correct, it implies that our observation of $\Delta^{66}Zn_{coral-sw} \approx 0\text{‰}$ is fortuitous, reflecting the balance between two approximately equal and opposite isotopic fractionations: one between aqueous species (including organic ligands) in the ECF (driving Zn^{2+} to low $\delta^{66}Zn$ values), and the other linked to sorption of heavy Zn and its incorporation into coral aragonite. As yet, while there are constraints on Zn sorption onto calcite, the mechanism and Zn isotope fractionation of sorption and incorporation in aragonite

is unknown.

Finally, variable coral calcification efficiency, suggested above as a means to explain variable D_{Zn} (and D_{Cu}) values, may also have implications for coral Zn and Cu isotope compositions. For example, if the isotope fractionation factor varies with aragonite precipitation rate, or if a constant (non-zero) fractionation factor is combined with calcification following a Rayleigh distillation trend, coral isotopic compositions should evolve during calcification. However, in the data presented here, no clear trend is resolved between Zn/Ca or Cu/Ca and their respective isotopic systems (Fig. 5). We also observe that Zn/Ca ratios vary by a factor of two for cleaned sub-samples of the glacial-age Sars Seamount coral, with no associated variability in $\delta^{66}Zn$ (Fig. 4). Taken together, these observations support a small $\Delta^{66}Zn_{\text{coral-sw}}$ fractionation factor.

Overall, a rather complex picture emerges, in which aqueous speciation in the ECF, as well as the mechanism of sorption and/or incorporation of Zn (and Cu) into aragonite, could both play a role in determining coral isotopic compositions. Neither aspect is well understood, and both merit further detailed study. It is noteworthy that the Zn isotope compositions of diverse types of shallow water carbonates exhibit more variability (-0.56 to $+1.11\%$; Zhao et al., 2021) than the data presented here, perhaps in part as a result of the mechanisms outlined above. These authors also suggest kinetic effects as a possible mechanism to explain the observed isotopic variability. We do not see evidence for kinetic effects in the coral dataset, perhaps due to the slow growth rates of cold-water corals (e.g., Adkins et al., 2004). Two recent Zn isotope studies on shallow-water zooxanthellate corals also observed variability from ~ 0 to $+0.6\%$, which they attributed to temperature and photosynthetic effects (Ferrier-Pagès et al., 2018; Xiao et al., 2020), neither of which are relevant factors for cold-water corals. Indeed, we find that cold-water corals appear to reliably record seawater $\delta^{66}Zn$ values. Recommendations for future work include expanding the cold-water coral sample set, micro-analytical studies of spatial variability in individual corals, and experimental studies on isotopic fractionation in aragonite, both with and without organic ligands.

5. Conclusions and outlook for cold-water coral $\delta^{66}Zn$ values as a palaeoceanographic tracer

In summary, we show that thorough physical and chemical cleaning of cold-water corals effectively removes authigenic and detrital Zn- and Cu-containing phases, allowing isotopic analysis of the coral aragonite. We find significant interspecies variability in the partitioning behaviour of Zn and Cu in cold-water corals, and notable intra-specimen variability in Zn/Ca ratios. Aqueous speciation and coral calcification efficiency are considered likely drivers of this variability.

We focus on the palaeoceanographic potential of Zn isotope compositions in cold-water corals, due to the greater availability of seawater and experimental data in the literature for Zn compared to Cu. Somewhat unexpectedly given its variable partitioning behaviour, interspecies and intra-specimen Zn/Ca variability is not associated with variability in $\delta^{66}Zn$ values. To a first order, cold-water corals appear to record ambient seawater $\delta^{66}Zn$ values without isotope fractionation, suggesting their utility as an archive of past seawater Zn isotope compositions.

It is therefore conceivable that cold-water corals could be employed to trace past changes in whole oceanic Zn and Cu mass balance. In effect, cold-water corals from the intermediate and deep ocean record whole ocean isotopic compositions, given that the deep ocean is largely isotopically homogeneous (at least in the modern day) and contains over 95% of the total oceanic Zn inventory. At steady state, the whole ocean isotopic composition is a balance of the isotopic composition of the inputs ($\delta^{66}Zn_{\text{input}}$) and any isotopic fractionation on output to sediments (Δ_{output}):

$$\delta^{66}Zn_{\text{ocean}} = \delta^{66}Zn_{\text{input}} - \Delta_{\text{output}} \quad (8)$$

The major sedimentary output fluxes for Zn are Fe-Mn (hydr)oxides and organic-rich sediments (Little et al., 2014, 2016), whereas removal to carbonates is negligible and does not significantly impact the oceanic mass balance. As a result, Zn isotope compositions of cold-water corals should reflect changes in whole ocean Zn cycling on timescales comparable to its ocean residence time (estimated Zn $\tau_{\text{res}} = 3-8$ kyr, Little et al., 2016; Roshan et al., 2016).

The dataset of Zn and Cu isotopes on glacial-age corals presented here comprises only four samples, which precludes firm interpretations. Nonetheless, their $\delta^{66}Zn$ and $\delta^{65}Cu$ values generally overlap with Holocene corals and modern seawater from their respective settings, suggesting only limited glacial-interglacial changes in the deep ocean Zn and Cu budgets. It is notable, however, that the two North Atlantic corals have more positive $\delta^{66}Zn$ values ($+0.79\%$, $+0.67\%$) than the corals from the Southern Ocean and the Tasman Sea ($+0.37\%$, $+0.38\%$), hinting at past spatial variability, such as a possible change in the isotopic composition of the northern-sourced water mass endmember on glacial-interglacial timescales.

Finally, we emphasise that archives from shallow water depths are likely to be most sensitive to recording past changes in oceanic Zn cycling. The pioneering study of Pichat et al. (2003) analysed $\delta^{66}Zn$ values in the leachable carbonate fraction of a Pacific sediment core spanning the last 180 kyr. This record exhibits high frequency variability and a long-term trend towards lighter Zn isotope compositions over this interval (Pichat et al., 2003). Since the sediment core is primarily made up of coccoliths, these variations were interpreted in terms of changes in the Zn isotope composition of the surface ocean. By constraining any past changes in the whole ocean mass balance of Zn, a comparable cold-water coral record from deeper water depths would aid in the interpretation of such surface water variability. Future cold-water coral studies with better spatial and temporal coverage should enable a more detailed investigation of past changes in the oceanic Zn cycle.

Declaration of Competing Interest

The authors declare that they have no known competing financial interests or personal relationships that could have appeared to influence the work reported in this paper.

Acknowledgements

We would like to acknowledge Matthew Clarkson and an anonymous reviewer for thoughtful comments on a previous version of this manuscript. Many thanks to Katharina Kreissig and Barry Coles for maintaining the smooth running of the MAGIC labs at Imperial, and to Derek Vance for the use of the Neptune at ETH. Thanks also to Sophie Hines, who sub-sampled New England Seamount corals from the Adkins collection and to Tristan Horner, who provided valuable insights early on in the development of this project. This research was supported by a Leverhulme Trust early career fellowship to SHL (ECF-2014-615). DJW and Tvdf acknowledge support from the Natural Environment Research Council (NE/N001141/1) and a NERC independent research fellowship to DJW (NE/T011440/1). SHL is currently supported by a NERC independent research fellowship (NE/P018181/2).

Appendix A. Supplementary data

Supplementary data to this article can be found online at <https://doi.org/10.1016/j.chemgeo.2021.120304>.

References

- Adkins, J.F., Boyle, E.A., Curry, W.B., Lutring, A., 2003. Stable isotopes in deep-sea corals and a new mechanism for "vital effects". *Geochim. Cosmochim. Acta.* [https://doi.org/10.1016/S0016-7037\(00\)01203-6](https://doi.org/10.1016/S0016-7037(00)01203-6).

- Adkins, J.F., Henderson, G.M., Wang, S.-L., O'Shea, S., Mokadem, F., 2004. Growth rates of the deep-sea scleractinia *Desmophyllum cristagalli* and *Enallopsammia rostrata*. *Earth Planet. Sci. Lett.* 227, 481–490.
- Albarède, F., 2004. The stable isotope geochemistry of copper and zinc. *Rev. Mineral. Geochem.* 55, 409–427. <https://doi.org/10.2138/gsrng.55.1.409>.
- Al-Horani, F.A., Al-Moghrabi, S.M., De Beer, D., 2003. The mechanism of calcification and its relation to photosynthesis and respiration in the scleractinian coral *Galaxea fascicularis*. *Mar. Biol.* 142, 419–426.
- Allemand, D., Ferrier-Pagès, C., Furla, P., Houlbrèque, F., Puverel, S., Reynaud, S., Tambutté, É., Tambutté, S., Zoccola, D., 2004. Biomineralisation in reef-building corals: from molecular mechanisms to environmental control. *Comptes Rendus - Palevol.* 3, 453–467. <https://doi.org/10.1016/j.crpv.2004.07.011>.
- Anagnostou, E., Sherrill, R.M., Gagnon, A., LaVigne, M., Field, M.P., McDonough, W.F., 2011. Seawater nutrient and carbonate ion concentrations recorded as P/Ca, Ba/Ca, and U/Ca in the deep-sea coral *Desmophyllum dianthus*. *Geochim. Cosmochim. Acta* 75, 2529–2543. <https://doi.org/10.1016/j.gca.2011.02.019>.
- Andersen, M.B., Vance, D., Archer, C., Anderson, R.F., Ellwood, M.J., Allen, C.S., 2011. The Zn abundance and isotopic composition of diatom frustules, a proxy for Zn availability in ocean surface seawater. *Earth Planet. Sci. Lett.* 301, 137–145. <https://doi.org/10.1016/j.epsl.2010.10.032>.
- Archer, C., Vance, D., 2004. Mass discrimination correction in multiple-collector plasma source mass spectrometry: an example using Cu and Zn isotopes. *J. Anal. At. Spectrom.* 19, 656. <https://doi.org/10.1039/b315853e>.
- Arnold, T., Schönbacher, M., Rehkämper, M., Dong, S., Zhao, F.J., Kirk, G.J.D., Coles, B. J., Weiss, D.J., 2010. Measurement of zinc stable isotope ratios in biogeochemical matrices by double-spike MC-ICPMS and determination of the isotope ratio pool available for plants from soil. *Anal. Bioanal. Chem.* 398, 3115–3125. <https://doi.org/10.1007/s00216-010-4231-5>.
- Bacconnais, I., Rouxel, O., Dulaquais, G., Boye, M., 2019. Determination of the copper isotope composition of seawater revisited: a case study from the Mediterranean Sea. *Chem. Geol.* 511, 465–480. <https://doi.org/10.1016/j.chemgeo.2018.09.009>.
- Bigalke, M., Weyer, S., Kobza, J., Wilcke, W., 2010. Stable Cu and Zn isotope ratios as tracers of sources and transport of Cu and Zn in contaminated soil. *Geochim. Cosmochim. Acta* 74, 6801–6813. <https://doi.org/10.1016/j.gca.2010.08.044>.
- Boyle, E.A., 1981. Cadmium, zinc, copper, and barium in foraminifera tests. *Earth Planet. Sci. Lett.* 53, 11–35. [https://doi.org/10.1016/0012-821X\(81\)90022-4](https://doi.org/10.1016/0012-821X(81)90022-4).
- Boyle, E.A., Sclater, F.R., Edmond, J.M., 1977. The distribution of dissolved copper in the Pacific. *Earth Planet. Sci. Lett.* 37, 38–54. [https://doi.org/10.1016/0012-821X\(77\)90144-3](https://doi.org/10.1016/0012-821X(77)90144-3).
- Brahmi, C., Kopp, C., Domart-Coulon, I., Stolarski, J., Meibom, A., 2012. Skeletal growth dynamics linked to trace-element composition in the scleractinian coral *Pocillopora damicornis*. *Geochim. Cosmochim. Acta* 99, 146–158.
- Bridgestock, L.J., Williams, H., Rehkämper, M., Larnier, F., Giscard, M.D., Hammond, S., Coles, B., Andreasen, R., Wood, B.J., Theis, K.J., 2014. Unlocking the zinc isotope systematics of iron meteorites. *Earth Planet. Sci. Lett.* 400, 153–164.
- Bruland, K.W., 1980. Oceanographic distributions of cadmium, zinc, nickel and copper in the North Pacific. *Earth Planet. Sci. Lett.* 47, 176–198.
- Bruland, K.W., 1989. Complexation of zinc by natural organic ligands in the central North Pacific. *Limnol. Oceanogr.* 34, 269–285.
- Bruland, K.W., Middag, R., Lohan, M.C., 2013. Controls of trace metals in seawater. In: *Treatise on Geochemistry*, 2nd ed. Elsevier Ltd. <https://doi.org/10.1016/B978-0-08-095975-7.00602-1>.
- Bryan, S.P., Marchitto, T.M., 2010. Testing the utility of paleonutrient proxies Cd/Ca and Zn/Ca in benthic foraminifera from thermocline waters. *Geochim. Geophys. Geosyst.* 11. <https://doi.org/10.1029/2009GC002780> n/a-n/a.
- Brzezinski, M.A., Pride, C.J., Franck, V.M., Sigman, D.M., Sarmiento, J.L., Matsumoto, K., Gruber, N., Rau, G.H., Coale, K.H., 2002. A switch from Si (OH) 4 to NO₃– depletion in the glacial Southern Ocean. *Geophys. Res. Lett.* 29, 1–5.
- Burke, A., 2012. Constraining Circulation Changes through the Last Deglaciation with Deep-sea Coral Radiocarbon and Sedimentary ²³¹Pa/²³⁰Th. MIT/WHOI.
- Case, D.H., Robinson, L.F., Auro, M.E., Gagnon, A.C., 2010. Environmental and biological controls on Mg and Li in deep-sea scleractinian corals. *Earth Planet. Sci. Lett.* 300, 215–225. <https://doi.org/10.1016/j.epsl.2010.09.029>.
- Chen, T., Robinson, L.F., Burke, A., Southon, J., Spooner, P., Morris, P.J., Ng, H.C., 2015. Synchronous centennial abrupt events in the ocean and atmosphere during the last deglaciation. *Science* (80). <https://doi.org/10.1126/science.aac6159>.
- Chen, T., Robinson, L.F., Beasley, M.P., Claxton, L.M., Andersen, M.B., Gregoire, L.J., Wadhams, J., Fornari, D.J., Harpp, K.S., 2016. Ocean mixing and ice-sheet control of seawater ²³⁴U/²³⁸U during the last deglaciation. *Science* (80). <https://doi.org/10.1126/science.aag1015>.
- Cheng, H., Adkins, J., Edwards, R.L., Boyle, E.A., 2000. U-Th dating of deep-sea corals. *Geochim. Cosmochim. Acta* 64, 2401–2416. [https://doi.org/10.1016/S0016-7037\(99\)00422-6](https://doi.org/10.1016/S0016-7037(99)00422-6).
- Clarkson, M.O., Müsing, K., Andersen, M.B., Vance, D., 2020. Examining pelagic carbonate-rich sediments as an archive for authigenic uranium and molybdenum isotopes using reductive cleaning and leaching experiments. *Chem. Geol.* 539, 119412. <https://doi.org/10.1016/j.chemgeo.2019.119412>.
- Coale, K.H., Bruland, K.W., 1988. Copper complexation in the Northeast Pacific. *Limnol. Oceanogr.* 33, 1084–1101.
- Cohen, A.L., McConnaughey, T.A., 2003. Geochemical perspectives on coral mineralization. *Rev. Mineral. Geochem.* 54, 151–187. <https://doi.org/10.2113/0540151>.
- Conway, T.M., John, S.G., 2014. The biogeochemical cycling of zinc and zinc isotopes in the North Atlantic Ocean. *Glob. Biogeochem. Cycles* 28, 1111–1128. <https://doi.org/10.1002/2014GB004862>. Received.
- Conway, T.M., John, S.G., 2015. The cycling of iron, zinc and cadmium in the North East Pacific Ocean - Insights from stable isotopes. *Geochim. Cosmochim. Acta* 164, 262–283. <https://doi.org/10.1016/j.gca.2015.05.023>.
- Crocket, J.H., Winchester, J.W., 1966. Coprecipitation of zinc with calcium carbonate. *Geochim. Cosmochim. Acta* 30, 1093–1109. [https://doi.org/10.1016/0016-7037\(66\)90119-0](https://doi.org/10.1016/0016-7037(66)90119-0).
- Crocket, K.C., Lambelet, M., van de Flierdt, T., Rehkämper, M., Robinson, L.F., 2014. Measurement of fossil deep-sea coral Nd isotopic compositions and concentrations by TIMS as NdO₂, with evaluation of cleaning protocols. *Chem. Geol.* 374–375, 128–140. <https://doi.org/10.1016/j.chemgeo.2014.03.011>.
- Cuif, J.P., Dauphin, Y., Berthet, P., Jegoudez, J., 2004. Associated water and organic compounds in coral skeletons: quantitative thermogravimetry coupled to infrared absorption spectrometry. *Geochim. Geophys. Geosyst.* 5, 1–9. <https://doi.org/10.1029/2004GC000783>.
- Cuif, J.-P., Dauphin, Y., Doucet, J., Salome, M., Susini, J., 2003. XANES mapping of organic sulfate in three scleractinian coral skeletons. *Geochim. Cosmochim. Acta* 67, 75–83.
- De Nooijer, L.J., Spero, H.J., Erez, J., Bijma, J., Reichart, G.J., 2014. Biomineralization in perforate foraminifera. *Earth-Sci. Res.* <https://doi.org/10.1016/j.earscirev.2014.03.013>.
- van Dijk, I., de Nooijer, L.J., Wolthers, M., Reichart, G.J., 2017. Impacts of pH and [CO₃–] on the incorporation of Zn in foraminiferal calcite. *Geochim. Cosmochim. Acta* 197, 263–277. <https://doi.org/10.1016/j.gca.2016.10.031>.
- Dong, S., Wasylenko, L.E., 2016. Zinc isotope fractionation during adsorption to calcite at high and low ionic strength. *Chem. Geol.* 447, 70–78.
- Druce, M., 2021. Expanding the Utility of the Zinc and Cadmium Stable Isotope Micronutrient Proxies, and Reconstructing Palaeo-Productivity through the Last Deglaciation. University of Otago.
- Elderfield, H., Bertram, C.J., Erez, J., 1996. A biomineralization model for the incorporation of trace elements into foraminiferal calcium carbonate. *Earth Planet. Sci. Lett.* 142, 409–423. [https://doi.org/10.1016/0012-821X\(96\)00105-7](https://doi.org/10.1016/0012-821X(96)00105-7).
- Ellwood, M.J., Van Den Berg, C.M.G., 2000. Zinc speciation in the Northeastern Atlantic Ocean. *Mar. Chem.* 68, 295–306. [https://doi.org/10.1016/S0304-4203\(99\)00085-7](https://doi.org/10.1016/S0304-4203(99)00085-7).
- Elzinga, E.J., Reeder, R.J., 2002. X-ray absorption spectroscopy study of Cu²⁺ and Zn²⁺ adsorption complexes at the calcite surface: implications for site-specific metal incorporation preferences during calcite crystal growth. *Geochim. Cosmochim. Acta* 66, 3943–3954. [https://doi.org/10.1016/S0016-7037\(02\)00971-7](https://doi.org/10.1016/S0016-7037(02)00971-7).
- Ferrier-Pagès, C., Sauzéat, L., Balter, V., 2018. Coral bleaching is linked to the capacity of the animal host to supply essential metals to the symbionts. *Global Change Biol.* 24 (7), 3145–3157.
- Elzinga, E.J., Rouff, A.A., Reeder, R.J., 2006. The long-term fate of Cu²⁺, Zn²⁺, and Pb²⁺ adsorption complexes at the calcite surface: an X-ray absorption spectroscopy study. *Geochim. Cosmochim. Acta* 70, 2715–2725. <https://doi.org/10.1016/j.gca.2006.02.026>.
- Finch, A.A., Allison, N., 2008. Mg structural state in coral aragonite and implications for the paleoenvironmental proxy. *Geophys. Res. Lett.* 35.
- van de Flierdt, T., Robinson, L.F., Adkins, J.F., 2010. Deep-sea coral aragonite as a recorder for the neodymium isotopic composition of seawater. *Geochim. Cosmochim. Acta* 74, 6014–6032. <https://doi.org/10.1016/j.gca.2010.08.001>.
- Fujii, T., Moynier, F., Blichert-Toft, J., Albarède, F., 2014. Density functional theory estimation of isotope fractionation of Fe, Ni, Cu, and Zn among species relevant to geochemical and biological environments. *Geochim. Cosmochim. Acta* 140, 553–576. <https://doi.org/10.1016/j.gca.2014.05.051>.
- Gabitov, R.I., Gaetani, G.A., Watson, E.B., Cohen, A.L., Ehrlich, H.L., 2008. Experimental determination of growth rate effect on U⁶⁺ and Mg²⁺ partitioning between aragonite and fluid at elevated U⁶⁺ concentration. *Geochim. Cosmochim. Acta* 72, 4058–4068.
- Gagnon, A.C., Adkins, J.F., Fernandez, D.P., Robinson, L.F., 2007. Sr/Ca and Mg/Ca vital effects correlated with skeletal architecture in a scleractinian deep-sea coral and the role of Rayleigh fractionation. *Earth Planet. Sci. Lett.* 261, 280–295. <https://doi.org/10.1016/j.epsl.2007.07.013>.
- Gagnon, A.C., Adkins, J.F., Erez, J., 2012. Seawater transport during coral biomineralization. *Earth Planet. Sci. Lett.* 329–330, 150–161. <https://doi.org/10.1016/j.epsl.2012.03.005>.
- Hasenfratz, A.P., Martínez-García, A., Jaccard, S.L., Vance, D., Wälle, M., Greaves, M., Haug, G.H., 2017. Determination of the Mg/Mn ratio in foraminiferal coatings: an approach to correct Mg/Ca temperatures for Mn-rich contaminant phases. *Earth Planet. Sci. Lett.* 457, 335–347. <https://doi.org/10.1016/j.epsl.2016.10.004>.
- Heller, M.I., Croot, P.L., 2015. Copper speciation and distribution in the Atlantic sector of the Southern Ocean. *Mar. Chem.* 173, 253–268.
- Hemsing, F., Hsieh, Y.-T., Bridgestock, L., Spooner, P.T., Robinson, L.F., Frank, N., Henderson, G.M., 2018. Barium isotopes in cold-water corals. *Earth Planet. Sci. Lett.* 491, 183–192.
- Hendry, K.R., Andersen, M.B., 2013. The zinc isotopic composition of siliceous marine sponges: investigating nature's sediment traps. *Chem. Geol.* 354, 33–41. <https://doi.org/10.1016/j.chemgeo.2013.06.025>.
- Ip, Y.K., Lim, A.L.L., Lim, R.W.L., 1991. Some properties of calcium-activated adenosine triphosphatase from the hermatypic coral *Galaxea fascicularis*. *Mar. Biol.* 111, 191–197.
- Jakuba, R.W., Saito, M.A., Moffett, J.W., Xu, Y., 2012. Dissolved zinc in the subarctic North Pacific and Bering Sea: its distribution, speciation, and importance to primary producers. *Glob. Biogeochem. Cycles* 26, 1–15. <https://doi.org/10.1029/2010GB004004>.
- John, S.G., Conway, T.M., 2014. A role for scavenging in the marine biogeochemical cycling of zinc and zinc isotopes. *Earth Planet. Sci. Lett.* 394, 159–167. <https://doi.org/10.1016/j.epsl.2014.02.053>.

- John, S.G., Geis, R.W., Saito, M.A., Boyle, E.A., 2007. Zinc isotope fractionation during high affinity and low-affinity zinc transport by the marine diatom *Thalassiosira oceanica*. *Limnol. Oceanogr.* 52, 2710–2714.
- John, S.G., Kunzmann, M., Townsend, E.J., Rosenberg, A.D., 2017. Zinc and cadmium stable isotopes in the geological record: a case study from the post-snowball Earth *Nuccaleena cap dolostone*. *Palaeogeogr. Palaeoclimatol. Palaeoecol.* 466, 202–208. <https://doi.org/10.1016/j.palaeo.2016.11.003>.
- John, S.G., Helgoe, J., Townsend, E., 2018. Biogeochemical cycling of Zn and Cd and their stable isotopes in the Eastern Tropical South Pacific. *Mar. Chem.* 201, 256–262. <https://doi.org/10.1016/j.marchem.2017.06.001>.
- Jouvin, D., Louvat, P., Juillot, F., Maréchal, C.N., Benedetti, M.F., 2009. Zinc isotopic fractionation: why organic matters. *Environ. Sci. Technol.* 43, 5747–5754. <https://doi.org/10.1021/es803012e>.
- Kitahara, M.V., Cairns, S.D., Miller, D.J., 2010a. Monophyletic origin of *Caryophyllia* (*Scleractinia*, *Caryophylliidae*), with descriptions of six new species. *Syst. Biodivers.* 8, 91–118.
- Kitahara, M.V., Cairns, S.D., Stolarski, J., Blair, D., Miller, D.J., 2010b. A comprehensive phylogenetic analysis of the *Scleractinia* (*Cnidaria*, *Anthozoa*) based on mitochondrial CO1 sequence data. *PLoS One* 5.
- Kitano, Y., Kanamori, N., Tokuyama, A., Comori, T., 1973. Factors controlling the trace-element contents of marine carbonate skeletons. In: *Proceeding of Symposium on Hydrogeochemistry and Biogeochemistry*, 484–499. The Clarke Co, Washington, DC.
- Kitano, Y., Okumura, M., Idogaki, M., 1980. Abnormal behaviors of copper (II) and zinc ions in parent solution at the early stage of calcite formation. *Geochem. J.* 14, 167–175. <https://doi.org/10.2343/geochemj.14.167>.
- Köbberich, M., Vance, D., 2017. Kinetic control on Zn isotope signatures recorded in marine diatoms. *Geochim. Cosmochim. Acta* 210, 97–113. <https://doi.org/10.1016/j.gca.2017.04.014>.
- Kunzmann, M., Halverson, G.P., Sossi, P.A., Raub, T.D., Payne, J.L., Kirby, J., 2013. Zn isotope evidence for immediate resumption of primary productivity after snowball Earth. *Geology* 41, 27–30. <https://doi.org/10.1130/G33422.1>.
- Lee, Y.J., Elzinga, E.J., Reeder, R.J., 2005. Cu(II) adsorption at the calcite-water interface in the presence of natural organic matter: Kinetic studies and molecular-scale characterization. *Geochim. Cosmochim. Acta* 69, 49–61. <https://doi.org/10.1016/j.gca.2004.06.015>.
- Lemaitre, N., de Souza, G.F., Archer, C., Wang, R.M., Planquette, H., Sarthou, G., Vance, D., 2020. Pervasive sources of isotopically light zinc in the North Atlantic Ocean. *Earth Planet. Sci. Lett.* 539, 116216. <https://doi.org/10.1016/j.epsl.2020.116216>.
- Liao, W.H., Takano, S., Yang, S.C., Huang, K.F., Sohrin, Y., Ho, T.Y., 2020. Zn isotope composition in the water column of the Northwestern Pacific Ocean: the importance of external sources. *Glob. Biogeochem. Cycles* 34, 1–18. <https://doi.org/10.1029/2019GB006379>.
- Little, S.H., Vance, D., Siddall, M., Gasson, E., 2013. A modeling assessment of the role of reversible scavenging in controlling oceanic dissolved Cu and Zn distributions. *Glob. Biogeochem. Cycles* 27, 780–791. <https://doi.org/10.1002/gbc.20073>.
- Little, S.H., Vance, D., Walker-Brown, C., Landing, W.M., 2014. The oceanic mass balance of copper and zinc isotopes, investigated by analysis of their inputs, and outputs to ferromanganese oxide sediments. *Geochim. Cosmochim. Acta* 125, 673–693. <https://doi.org/10.1016/j.gca.2013.07.046>.
- Little, S.H., Vance, D., McManus, J., Severmann, S., 2016. Key role of continental margin sediments in the oceanic mass balance of Zn and Zn isotopes. *Geology* 44, 207–210. <https://doi.org/10.1130/G37493.1>.
- Little, S.H., Vance, D., McManus, J., Severmann, S., Lyons, T.W., 2017. Copper isotope signatures in modern marine sediments. *Geochim. Cosmochim. Acta* 212, 253–273. <https://doi.org/10.1016/j.gca.2017.06.019>.
- Little, S.H., Archer, C., Milne, A., Schlosser, C., Achterberg, E.P., Lohan, M.C., Vance, D., 2018. Paired dissolved and particulate phase Cu isotope distributions in the South Atlantic. *Chem. Geol.* 502, 29–43. <https://doi.org/10.1016/j.chemgeo.2018.07.022>.
- Little, S.H., Munson, S., Prytkal, J., Coles, B.J., Hammond, S.J., Widdowson, M., 2019. Cu and Zn isotope fractionation during extreme chemical weathering. *Geochim. Cosmochim. Acta* 263, 85–107. <https://doi.org/10.1016/j.gca.2019.07.057>.
- Liu, S.A., Wu, H., Shen, S.Z., Jiang, G., Zhang, S., Lv, Y., Zhang, H., Li, S., 2017. Zinc isotope evidence for intensive magmatism immediately before the end-Permian mass extinction. *Geology* 45, 343–346. <https://doi.org/10.1130/G38644.1>.
- Lomitschka, M., Mangini, A., 1999. Precise Th/U-dating of small and heavily coated samples of deep sea corals. *Earth Planet. Sci. Lett.* 170, 391–401. [https://doi.org/10.1016/S0012-821X\(99\)00117-X](https://doi.org/10.1016/S0012-821X(99)00117-X).
- Marchitto, T.M., Broecker, W.S., 2006. Deep water mass geometry in the glacial Atlantic Ocean: a review of constraints from the paleonutrient proxy Cd/Ca. *Geochim. Geophys. Geosyst.* 7. <https://doi.org/10.1029/2006GC001323>.
- Marchitto, T.M., Curry, W.B., Oppo, D.W., 2000. Zinc concentrations in benthic foraminifera reflect seawater chemistry. *Paleoceanography* 15, 299–306.
- Marchitto, T.M., Lynch-Stieglitz, J., Hemming, S.R., 2005. Deep Pacific CaCO₃ compensation and glacial-interglacial atmospheric CO₂. *Earth Planet. Sci. Lett.* 231, 317–336. <https://doi.org/10.1016/j.epsl.2004.12.024>.
- Maréchal, C., Sheppard, S., 2002. Isotopic fractionation of Cu and Zn between chloride and nitrate solutions and malachite or smithsonite at 30 degrees and 50 degrees. *Geochim. Cosmochim. Acta* 66, A484.
- Maréchal, C.N., Télouk, P., Albarède, F., 1999. Precise analysis of copper and zinc isotopic compositions by plasma-source mass spectrometry. *Chem. Geol.* 156, 251–273. [https://doi.org/10.1016/S0009-2541\(98\)00191-0](https://doi.org/10.1016/S0009-2541(98)00191-0).
- Maréchal, C.N., Nicolas, E., Douchet, C., Albarède, F., 2000. Abundance of zinc isotopes as a marine biogeochemical tracer. *Geochim. Geophys. Geosyst.* 1. <https://doi.org/10.1029/1999GC000029> n/a-n/a.
- Margolin, A.R., Robinson, L.F., Burke, A., Waller, R.G., Scanlon, K.M., Roberts, M.L., Auro, M.E., van de Fliedert, T., 2014. Temporal and spatial distributions of cold-water corals in the Drake Passage: insights from the last 35,000 years. *Deep. Res. Part II Top. Stud. Oceanogr.* 99, 237–248. <https://doi.org/10.1016/j.dsr2.2013.06.008>.
- Marković, T., Manzoor, S., Humphreys-Williams, E., Kirk, G.J.D., Vilar, R., Weiss, D.J., 2017. Experimental determination of zinc isotope fractionation in complexes with the phytosiderophore 2'-deoxymugenic Acid (DMA) and its structural analogues, and implications for plant uptake mechanisms. *Environ. Sci. Technol.* 51, 98–107. <https://doi.org/10.1021/acs.est.6b00566>.
- Matsumoto, K., Sarmiento, J.L., Brzezinski, M.A., 2002. Silicic acid leakage from the Southern Ocean: a possible explanation for glacial atmospheric pCO₂. *Glob. Biogeochem. Cycles* 16, 1–5.
- Mavromatis, V., González, A.G., Dietzel, M., Schott, J., 2019. Zinc isotope fractionation during the inorganic precipitation of calcite – Towards a new pH proxy. *Geochim. Cosmochim. Acta* 244, 99–112. <https://doi.org/10.1016/j.gca.2018.09.005>.
- McBride, M.B., 1981. Forms and distribution of copper in solid and solution phases of soil. In: Loneragan, J.F., Robson, A.D., Graham, R.D. (Eds.), *Copper in Soils and Plants*. Academic Press, Australia.
- Meibom, A., Cuif, J.P., Houbreque, F., Mostefaoui, S., Dauphin, Y., Meibom, K.L., Dunbar, R., 2008. Compositional variations at ultra-structure length scales in coral skeleton. *Geochim. Cosmochim. Acta* 72, 1555–1569. <https://doi.org/10.1016/j.gca.2008.01.009>.
- Menadakis, M., Maroulis, G., Koutsoukos, P.G., 2007. A quantum chemical study of doped CaCO₃ (calcite). *Comput. Mater. Sci.* 38, 522–525.
- Menadakis, M., Maroulis, G., Koutsoukos, P.G., 2009. Incorporation of Mg²⁺, Sr²⁺, Ba²⁺ and Zn²⁺ into aragonite and comparison with calcite. *J. Math. Chem.* 46, 484–491. <https://doi.org/10.1007/s10910-008-9490-4>.
- Middag, R., de Baar, H.J.W., Bruland, K.W., 2019. The relationships between dissolved zinc and major nutrients phosphate and silicate along the GEOTRACES GA02 transect in the West Atlantic Ocean. *Glob. Biogeochem. Cycles*. <https://doi.org/10.1029/2018GB006034>.
- Moffett, J.W., Dupont, C., 2007. Cu complexation by organic ligands in the sub-arctic NW Pacific and Bering Sea. *Deep Sea Res. Part I Oceanogr. Res. Pap.* 54, 586–595. <https://doi.org/10.1016/j.dsr.2006.12.013>.
- Moynier, F., Vance, D., Fujii, T., Savage, P., 2017. The isotope geochemistry of zinc and copper. *Rev. Mineral. Geochem.* 82, 543–600. <https://doi.org/10.2138/rmg.2017.82.13>.
- Munsel, D., Kramar, U., Dissard, D., Nehrke, G., Berner, Z., Bijma, J., Reichart, G.-J., Neumann, T., 2010. Heavy metal uptake in foraminiferal calcite: results of multi-element culture experiments. *Biogeosci. Discuss.* 7, 953–977. <https://doi.org/10.5194/bgd-7-953-2010>.
- Nardelli, M.P., Malferrari, D., Ferretti, A., Bartolini, A., Sabbatini, A., Negri, A., 2016. Zinc incorporation in the miliolid foraminifer *Pseudotriloculina rotunda* under laboratory conditions. *Mar. Micropaleontol.* 126, 42–49. <https://doi.org/10.1016/j.marmicro.2016.06.001>.
- de Nooijer, L.J., Reichart, G.J., Dueñas-Bohórquez, A., Wolthers, M., Ernst, S.R., Mason, P.R.D., van der Zwaan, G.J., 2007. Copper incorporation in foraminiferal calcite: results from culturing experiments. *Biogeosci. Discuss.* 4, 961–991. <https://doi.org/10.5194/bgd-4-961-2007>.
- Pichat, S., Douchet, C., Albarède, F., 2003. Zinc isotope variations in deep-sea carbonates from the eastern equatorial Pacific over the last 175 ka. *Earth Planet. Sci. Lett.* 210, 167–178. [https://doi.org/10.1016/S0012-821X\(03\)00106-7](https://doi.org/10.1016/S0012-821X(03)00106-7).
- Pratt, N., Chen, T., Li, T., Wilson, D.J., van de Fliedert, T., Little, S.H., Taylor, M.L., Robinson, L.F., Rogers, A.D., Santodomingo, N., 2019. Temporal distribution and diversity of cold-water corals in the Southwest Indian Ocean over the past 25,000 years. *Deep. Res. Part I Oceanogr. Res. Pap.* 149. <https://doi.org/10.1016/j.dsr.2019.05.009>.
- Reeder, R.J., Lambie, G.M., Northrup, P.A., 1999. XAFS study of the coordination and local relaxation around Co²⁺, Zn²⁺, Pb²⁺, and Ba²⁺ trace elements in calcite. *Am. Mineral.* 84, 1049–1060.
- Richon, C., Tagliabue, A., 2019. Insights into the major processes driving the global distribution of copper in the ocean from a global model. *Glob. Biogeochem. Cycles* 33, 1594–1610. <https://doi.org/10.1029/2019GB006280>.
- Rimstidt, J.D., Balog, A., Webb, J., 1998. Distribution of trace elements between carbonate minerals and aqueous solutions. *Geochim. Cosmochim. Acta* 62, 1851–1863. [https://doi.org/10.1016/S0016-7037\(98\)00125-2](https://doi.org/10.1016/S0016-7037(98)00125-2).
- Roberts, J.M., Wheeler, A., Freiwald, A., Cairns, S., 2009. *Cold-Water Corals: The Biology and Geology of Deep-Sea Coral Habitats*. Cambridge University Press.
- Robinson, L.F., Adkins, J., Scheirer, D., Fernandez, D.P., Gagnon, A.C., Waller, R., 2007. Deep-sea scleractinian coral age and depth distributions in the NW Atlantic for the last 225 thousand years. *Bull. Mar. Sci.* 81, 371–391.
- Robinson, L.F., Adkins, J.F., Frank, N., Gagnon, A.C., Prouty, N.G., Brendan Roark, E., van de Fliedert, T., 2014. The geochemistry of deep-sea coral skeletons: a review of vital effects and applications for paleoceanography. *Deep. Res. Part II Top. Stud. Oceanogr.* 99, 184–198. <https://doi.org/10.1016/j.dsr2.2013.06.005>.
- Rollion-Bard, C., Blamart, D., Cuif, J.-P., Dauphin, Y., 2010. In situ measurements of oxygen isotopic composition in deep-sea coral, *Lophelia pertusa*: re-examination of the current geochemical models of biomineralization. *Geochim. Cosmochim. Acta* 74, 1338–1349.
- Rollion-Bard, C., Blamart, D., Trebosch, J., Tricot, G., Mussi, A., Cuif, J.-P., 2011. Boron isotopes as pH proxy: a new look at boron speciation in deep-sea corals using 11B MAS NMR and EELS. *Geochim. Cosmochim. Acta* 75, 1003–1012. <https://doi.org/10.1016/j.gca.2010.11.023>.
- Roshan, S., Wu, J., 2015. The distribution of dissolved copper in the tropical-subtropical North Atlantic across the GEOTRACES GA03 transect. *Mar. Chem.* 176, 189–198. <https://doi.org/10.1016/j.marchem.2015.09.006>.

- Roshan, S., Wu, J., Jenkins, W.J., 2016. Long-range transport of hydrothermal dissolved Zn in the tropical South Pacific. *Mar. Chem.* 183, 25–32. <https://doi.org/10.1016/j.marchem.2016.05.005>.
- Ryan, B.M., Kirby, J.K., Degryse, F., Scheiderich, K., McLaughlin, M.J., 2014. Copper isotope fractionation during equilibration with natural and synthetic ligands. *Environ. Sci. Technol.* 48, 8620–8626. <https://doi.org/10.1021/es500764x>.
- Samanta, M., Ellwood, M.J., Sinoir, M., Hassler, C.S., 2017. Dissolved zinc isotope cycling in the Tasman Sea, SW Pacific Ocean. *Mar. Chem.* 192, 1–12. <https://doi.org/10.1016/j.marchem.2017.03.004>.
- Sarmiento, J.L., Gruber, N., Brzezinski, M.A., Dunne, J.P., 2004. High-latitude controls of thermocline nutrients and low latitude biological productivity. *Nature* 427, 56–60.
- Schlitzer, R., Anderson, R.F., Dodas, E.M., Lohan, M., Geibert, W., Tagliabue, A., Bowie, A., Jeandel, C., Maldonado, M.T., Landing, W.M., Cockwell, D., Abadie, C., Abouchami, W., Achterberg, E.P., Agather, A., Aguiar-Islas, A., van Aken, H.M., Andersen, M., Archer, C., Auro, M., de Baar, H.J.J., Baars, O., Baker, A.R., Bakker, K., Basak, B., Baskaran, M., Bates, N.R., Bauch, D., van Beek, P., Behrens, M.K., Black, E., Bluhm, K., Bopp, L., Bouman, H., Bowman, K., Bown, J., Boyd, P., Boyle, M., Boyle, E.A., Branell, P., Bridgestock, L., Brissebrat, G., Browning, T., Bruland, K.W., Brumsack, H.-J., Brzezinski, M., Buck, C.S., Buck, K.N., Buesseler, K., Bull, A., Butler, E., Cai, P., Mor, P.C., Cardinal, D., Carlson, C., Carrasco, G., Casacuberta, N., Casciotti, K.L., Castrillejo, M., Chamizo, E., Chance, R., Charette, M. A., Chaves, J.E., Cheng, H., Chever, M., Christl, M., Church, T.M., Closset, I., Colman, A., Conway, T.M., Cossa, D., Croot, P., Cullen, J.T., Cutter, G.A., Daniels, C., Dehairs, F., Deng, F., Dieu, H.T., Duggan, B., Dulaquais, G., Dumoussaud, C., Echevigo-Sanz, Y., Edwards, R.L., Ellwood, M., Fahrbach, E., Fitzsimmons, J.N., Russell Flegel, A., Fleisher, M.Q., van de Fliedert, T., Frank, M., Friedrich, J., Fripiat, F., Fröllje, H., Galer, S.J.G., Gamo, T., Ganeshram, R.S., Garcia-Orellana, J., Garcia-Solsona, E., Gault-Ringold, M., George, E., Gerringa, L.J.A., Godoy, J.M., Goldstein, S.L., Gonzalez, S.R., Grissom, K., Hammerschmidt, C., Hartman, A., Hassler, C.S., Hathorne, E.C., Hattala, M., Hawco, N., Hayes, C.T., Heimbürger, L.-E., Helgoe, J., Heller, M., Henderson, G.M., Henderson, P.B., van Heuven, S., Ho, P., Horner, T.J., Hsieh, Y.-T., Huang, K.-F., Humphreys, M.P., Ishiki, K., Jacquot, J.E., Janssen, D.J., Jenkins, W.J., John, S., Jones, E.M., Jones, J. L., Kadko, D.C., Kayser, R., Kenna, T.C., Khondoker, R., Kim, T., Kipp, L., Klar, J.K., Klunder, M., Kretschmer, S., Kumamoto, Y., Laan, P., Labatut, M., Lacan, F., Lam, P. J., Lambelet, M., Lamborg, C.H., Le Moigne, F.A.C., Le Roy, E., Lechtenfeld, O.J., Lee, J.-M., Lherminier, P., Little, S., López-Lora, M., Lu, Y., Masque, P., Mawji, E., McClain, C.R., Measures, C., Mehic, S., Barraqueta, J.-L.M., van der Merwe, P., Middag, R., Mieruch, S., Milne, A., Minami, T., Moffett, J.W., Moncoiffe, G., Moore, W.S., Morris, P.J., Morton, P.L., Nakaguchi, Y., Nakayama, N., Niedermiller, J., Nishioka, J., Nishiuchi, A., Noble, A., Obata, H., Ober, S., Onhemus, D.C., van Ooijen, J., O'Sullivan, J., Owens, S., Pahnke, K., Paul, M., Pavia, F., Pena, L.D., Peters, B., Planchon, F., Planquette, H., Pradoux, C., Puigcorbó, V., Quay, P., Queroue, J., Radic, A., Rauschenberg, S., Rehkämper, M., Rember, R., Remenyi, T., Resing, J.A., Rickli, J., Rigaud, S., Rijkenberg, M.J.A., Rintoul, S., Robinson, L.F., Roca-Martí, M., Rodellas, V., Roeske, T., Rolison, J.M., Rosenberg, M., Roshan, S., Rutgers van der Loeff, M.M., Ryabenko, E., Saito, M.A., Salt, L.A., Sanial, V., Sarthou, G., Schallenberg, C., Schauer, U., Scher, H., Schlosser, C., Schmetzger, B., Scott, P., Sedwick, P.N., Semiletov, I., Shelley, R., Sherrill, R.M., Shiller, A.M., Sigman, D.M., Singh, S.K., Slagter, H.A., Slater, E., Smethie, W.M., Snaith, H., Sohrin, Y., Sohst, B., Sonke, J.E., Speich, S., Steinfeldt, R., Stewart, G., Stichel, T., Stirling, C.H., Stutsman, J., Swarr, G.J., Swift, J.H., Thomas, A., Thorne, K., Till, C.P., Till, R., Townsend, A.T., Townsend, E., Tuenera, R., Twining, B.S., Vance, D., Velazquez, S., Venchiarutti, C., Villa-Alfageme, M., Vivanos, S.M., Voelker, A.H.L., Wake, B., Warner, M.J., Watson, R., van Weerlee, E., Alexandra Weigand, M., Weinstein, Y., Weiss, D., Wisotzki, A., Woodward, E.M.S., Wu, J., Wu, Y., Wuttig, K., Wyatt, N., Xiang, Y., Xie, R.C., Xue, Z., Yoshikawa, H., Zhang, J., Zhang, P., Zhao, Y., Zheng, L., Zheng, X.-Y., Zieringer, M., Zimmer, L.A., Ziveri, P., Zunino, P., Zurbrick, C., 2018. The GEOTRACES Intermediate Data Product 2017. *Chem. Geol.* <https://doi.org/10.1016/j.chemgeo.2018.05.040>.
- Sevilgen, D.S., Venn, A.A., Hu, M.Y., Tambutté, E., de Beer, D., Planas-Bielsa, V., Tambutté, S., 2019. Full in vivo characterization of carbonate chemistry at the site of calcification in corals. *Sci. Adv.* 5, eaau7447.
- Shen, G.T., Boyle, E.A., 1988. Determination of lead, cadmium and other trace metals in annually-banded corals. *Chem. Geol.* 67, 47–62. [https://doi.org/10.1016/0009-2541\(88\)90005-8](https://doi.org/10.1016/0009-2541(88)90005-8).
- Sieber, M., Conway, T.M., de Souza, G.F., Hassler, C.S., Ellwood, M.J., Vance, D., 2020. Cycling of zinc and its isotopes across multiple zones of the Southern Ocean: insights from the Antarctic circumnavigation expedition. *Geochim. Cosmochim. Acta* 268, 310–324. <https://doi.org/10.1016/j.gca.2019.09.039>.
- Siebert, C., Nägler, T.F., von Blanckenburg, F., Kramers, J.D., 2003. Molybdenum isotope records as a potential new proxy for paleoceanography. *Earth Planet. Sci. Lett.* 211, 159–171. [https://doi.org/10.1016/S0012-821X\(03\)00189-4](https://doi.org/10.1016/S0012-821X(03)00189-4).
- Sigman, D.M., Hain, M.P., Haug, G.H., 2010. The polar ocean and glacial cycles in atmospheric CO₂ concentration. *Nature* 466, 47–55. <https://doi.org/10.1038/nature09149>.
- Smrzka, D., Zwicker, J., Bach, W., Feng, D., Himmler, T., Chen, D., Peckmann, J., 2019. The behavior of trace elements in seawater, sedimentary pore water, and their incorporation into carbonate minerals: a review. *Facies*. <https://doi.org/10.1007/s10347-019-0581-4>.
- Sokolov, S., Rintoul, S.R., 2009. Circumpolar structure and distribution of the antarctic circumpolar current fronts: 1. Mean 98 circumpolar paths. *J. Geophys. Res. Ocean.* <https://doi.org/10.1029/2008JC005108>.
- de Souza, G.F., Khatiwala, S.P., Hain, M.P., Little, S.H., Vance, D., 2018. On the origin of the marine zinc-silicon correlation. *Earth Planet. Sci. Lett.* 492, 22–34. <https://doi.org/10.1016/j.epsl.2018.03.050>.
- Spooner, P.T., Robinson, L.F., Hemsing, F., Morris, P., Stewart, J.A., 2018. Extended calibration of cold-water coral Ba/Ca using multiple genera and co-located measurements of dissolved barium concentration. *Chem. Geol.* 499, 100–110. <https://doi.org/10.1016/j.chemgeo.2018.09.012>.
- Sweere, T.C., Dickson, A.J., Jenkyns, H.C., Porcelli, D., Elrick, M., van den Boorn, S.H.J.M., Henderson, G.M., 2018. Isotopic evidence for changes in the zinc cycle during Oceanic Anoxic event 2 (late cretaceous). *Geology* 46, 463–466. <https://doi.org/10.1130/G40226.1>.
- Takano, S., Tanimizu, M., Hirata, T., Sohrin, Y., 2014. Isotopic constraints on biogeochemical cycling of copper in the ocean. *Nat. Commun.* 5, 5663. <https://doi.org/10.1038/ncomms6663>.
- Temmam, M., Paquette, J., Vali, H., 2000. Mn and Zn incorporation into calcite as a function of chloride aqueous concentration. *Geochim. Cosmochim. Acta* 64, 2417–2420. [https://doi.org/10.1016/S0016-7037\(00\)00375-6](https://doi.org/10.1016/S0016-7037(00)00375-6).
- Thiagarajan, N., Gerlach, D., Roberts, M.L., Burke, A., McNichol, A., Jenkins, W.J., Subhas, A.V., Thresher, R.E., Adkins, J.F., 2013. Movement of deep-sea coral populations on climatic timescales. *Paleoceanography* 28, 227–236. <https://doi.org/10.1002/palo.20023>.
- Thompson, C.M., Ellwood, M.J., 2014. Dissolved copper isotope biogeochemistry in the Tasman Sea, SW Pacific Ocean. *Mar. Chem.* 165, 1–9. <https://doi.org/10.1016/j.marchem.2014.06.009>.
- Vance, D., Little, S.H., De Souza, G.F., Khatiwala, S., Lohan, M.C., Middag, R., 2017. Silicon and zinc biogeochemical cycles coupled through the Southern Ocean. *Nat. Geosci.* 10, 202–206. <https://doi.org/10.1038/ngeo2890>.
- Vance, D., de Souza, G.F., Zhao, Y., Cullen, J.T., Lohan, M.C., 2019. The relationship between zinc, its isotopes, and the major nutrients in the North-East Pacific. *Earth Planet. Sci. Lett.* 525, 115748. <https://doi.org/10.1016/j.epsl.2019.115748>.
- Veeramani, H., Eagling, J., Jamieson-Hanes, J.H., Kong, L., Ptacek, C.J., Blowes, D.W., 2015. Zinc isotope fractionation as an indicator of geochemical attenuation processes. *Environ. Sci. Technol. Lett.* 2, 314–319. <https://doi.org/10.1021/acs.estlett.5b00273>.
- Wang, R.M., Archer, C., Bowie, A.R., Vance, D., 2018. Zinc and nickel isotopes in seawater from the Indian Sector of the Southern Ocean: the impact of natural iron fertilization versus Southern Ocean hydrography and biogeochemistry. *Chem. Geol.* 1–13. <https://doi.org/10.1016/j.chemgeo.2018.09.010>.
- Weber, T., John, S., Tagliabue, A., DeVries, T., 2018. Biological uptake and reversible scavenging of zinc in the global ocean. *Science* (80) 361, 72–76. <https://doi.org/10.1126/science.aap8532>.
- Wilson, D.J., Crockett, K.C., Van De Fliedert, T., Robinson, L.F., Adkins, J.F., 2014. Dynamic intermediate ocean circulation in the North Atlantic during Heinrich Stadial 1: a radiocarbon and neodymium isotope perspective. *Paleoceanography* 29, 1072–1093. <https://doi.org/10.1002/2014PA002674>.
- Wilson, D.J., van de Fliedert, T., Adkins, J.F., 2017. Lead isotopes in deep-sea coral skeletons: ground-truthing and a first deglacial Southern Ocean record. *Geochim. Cosmochim. Acta* 204, 350–374.
- Xiao, H., Deng, W., Wei, G., Chen, J., Zheng, X., Shi, T., Chen, X., Wang, C., Liu, X., Zeng, T., 2020. A pilot study on zinc isotopic compositions in shallow-water coral skeletons. *Geochim. Geophys. Geosyst.* <https://doi.org/10.1029/2020gc009430>.
- Yu, J., Elderfield, H., Greaves, M., Day, J., 2007. Preferential dissolution of benthic foraminiferal calcite during laboratory reductive cleaning. *Geochim. Geophys. Geosyst.* 8. <https://doi.org/10.1029/2006GC001571>.
- Zhao, M., Tarhan, L.G., Zhang, Y., Hood, A., Asael, D., Reid, R.P., Planavsky, N.J., 2021. Evaluation of shallow-water carbonates as a seawater zinc isotope archive. *Earth Planet. Sci. Lett.* 553, 116599. <https://doi.org/10.1016/j.epsl.2020.116599>.
- Zhao, Y., Vance, D., Abouchami, W., de Baar, H.J.W., 2014. Biogeochemical cycling of zinc and its isotopes in the Southern Ocean. *Geochim. Cosmochim. Acta* 125, 653–672. <https://doi.org/10.1016/j.gca.2013.07.045>.